Fractal Dust Growth in the Protoplanetary Disk

Nakamura, Ryosuke

(Degree)
博士（理学）

(Date of Degree)
1996-03-31

(Date of Publication)
2015-02-24

(Resource Type)
doctoral thesis

(Report Number)
甲1547

(JaLCDOI)
https://doi.org/10.11501/3116895

(URL)
https://hdl.handle.net/20.500.14094/D1001547

博士論文

Fractal Dust Growth in the Protoplanetary Disk

平成8年1月

神戸大学大学院自然科学研究科

中村　良介

Ryosuke Nakamura

博士論文

Fractal Dust Growth in the Protoplanetary Disk

(原始惑星系円盤におけるフラクタルダスト成長)

Graduate School of Science and Technology
Kobe University, Nada 657, JAPAN

930D828N　Ryosuke NAKAMURA

Contents

Abstract

Main purpose of this paper is to examine the effect of the realistic geometry of dust aggregates on the evolution of protoplanetary disks. To begin with, two simple models for the grain coagulation process, i.e., ballistic particle-cluster aggregation (BPCA) and ballistic cluster-cluster aggregation (BCCA) are presented. These simple models demonstrate the remarkable influence of the growth kinetics on the geometry of the aggregates.

Subsequently,computer simulations of the collisions of gas molecules with fluffy aggregates has been carried out to estimate the drag force in the free molecular regime. The correlation between the rate of molecular collision and the efficiency momentum transfer is taken into account explicitly in our new computational framework. Quasi Monte Carlo method (QMC) made it possible to perform multivariate integrations with sufficient accuracies. We show that the gas drag force on fluffy aggregates can be approximated by that on area-equivalent sphere in a wide range of relative velocity of the aggregate to the ambient gas. The deviation from this approximation is weakly dependent on S, the relative velocity of the aggregate normalized by mean thermal velocity of the gas, and the size/structure of the aggregate,but less than 25 % for all cases investigated in the present work. give rise to the anisotropic drag force for $S >> 1$.

Chapter 3 investigates Smoluchowski's coagulation equation that govern the dynamics of spatially homogeneous particulate systems undergoing coagulation. First, the physical and mathematical basis of the equation is discussed. Among several algorithms to solve the coagulation equation, Wetherill's scheme has been selected because it provides us accurate results with modest computational cost. Several test calculations for exactly solvable collision kernels have shown the excellent agreement with the analytical formulae. Another advantage of this algorithm is the capability to follow "Runaway Growth" or "Gellation" of the largest body in the system. Related to this topic, previous analytical results concerning the scaling properties of coagulation equation are overviewed. We find that the values of several homogenity indices are quite useful to predict the behaviour of the size distribution qualitatively. Moreover, Monte Carlo simulations have been performed to investigate the time development of the size distribution and the geometry of each aggregate simultaneously. "Topping" technique is employed to increase the total particle number in the system and to reduce the computation time. It is found that the clusters formed by these simulations have porous and fluffy structures and their irregular shapes are characterized with a fractal dimension. The value of fractal dimension is appoximately 2 independent of the detail of the collision kernel

Combining the results of previous chapters, the growth of fratal dust aggregates is examined in this final chapter. For thermal coagulation, the growth speed of fractal aggregates becomes faster than that for compact sphere because the cross section is much larger compared with the mass-equivalent spherical particle and the relative velocity term is not affected by the geometry. In the case of turbulence-induced coagulation, the increase of the cross section is larger than the offset by the decrease of the relative velocity. As a result, the growth mode changes from power-law to exponential as a function of the unit time. On the other hand, the growth mode for coagulation driven by settling or radial drift remain exponential since the enhancement of the cross section is exactly cancelled by the decrease of the relative velocity. Comparing the time scale for sedimentation with

that for coagulation, we find that no mass-concentration to the midplane occurs for fractal growth. In addition, the transition of gas drag forces can cause runaway growth even for the growth of spherical compact particles. The onset of both phenomenon depends on the system size under consideration.

1 Introduction

Planet formation starts as a coagulation process of sub-micron sized interstellar grains or re-condensates in the protoplanetary disk. Much of the groundwork for modern research into early solar system was laid down by Safronov(1969). Also, Hayashi and co-workers in Kyoto group extensively investigated the process of planet formation (Hayashi et al. 1985). The "standard scenario" established by these authors consists of two separated stages, i.e.,

- stage 1: Planetesimal formation by gravitational instability (Sekiya 1983)
- stage 2: Planetesimal accumulation by mutual gravity (Lissauer and Stewart 1993)

In the former stage, dynamics of the solid matter is mainly controlled by the gas drag force whereas it is dominated by gravity in the latter stage. Two major reasons which made "standard scenario" popular are summarized as below.

1. The model doesn't require any specification of sticking mechanism other than gravity. Possibly, this is the most attractive feature of the model because it is rather difficult to join two particles, especially of sizes $\sim$ millimeter to kilometer. For smaller particles, inter-molecule interactions,such as van der Waals force, can serve as effective bonding, whereas gravity works for larger planetesimals. In the intermediate scale, however, the effective force for adhesion is comletely absent.

2. While both small grains and planetesimals can stay on the orbits stably, bodies of intermediate size, on which gas drag force and gravity exert to the same extent, rapidly spiral into the central star.(see,e.g. Adachi et al. and Weidenschilling 1988) In order to pile up small particles into planetesimals gradually, the growth must go through this unstable size. But, "standard scenario" avoids this difficulty by "Jumping" from dust to planetesimals with gravitational instability.

Although the simple picture seems quite appealing, the validity cannot be taken for granted simply because it provides an convenient bypass. This separation into two stage may be an artifact as pointed out by Weidenshiling and Cuzzi (1993). Most serious problem in the scenario is that even weak turbulence generated by the shear between the dust and gas layer would prevent the dust layer from further settling and reaching the critical density for gravitational instability(Weidenschilling and Cuzzi 1993). The continuous growth model by gradual coagulation has been proposed as an alternative path for planet formation. In both cases, we cannot avoid above-mentioned intricate problems concerning the particles of intermediate size.

Solid small particles have no effective force keep them spherical ,such as self-gravity for planetesimals or surface tension for liquid droplets. Indeed, both experimental (Praburam and Goree 1995) and theoretical (Ossenkopf 1993) studies suggest that the formation of fluffy aggregates is a general phenomenon in a variety of environment of astrophysical interest. Thus, it seems quite plausible that fluffy aggregates were produced in the protoplanetary disk. Direct evidence to support this conjecture has been obtained from interplanetary dust particles (IDPs) collected from the stratosphere (Brownlee 1987). A large fraction of IDPs, classified as chondritic porous type, are irregularly shaped aggregates consisting of smaller individual particles with sizes of $\sim 0.1\mu m$ and likely largely unmodified remnants of the planetary formation process. In this paper, we employ 'fractal' concept to describe the complex geometry of the realistic dust aggregates. As mentioned earlier, the dynamics of dust particle in the early stage is controlled by the interaction with the surrounding gas. Since gas drag force

in the free molecular regime crucially depends on the cross section, the geometry of the actual dust aggregates is expected to play an important role on the evolution of the disk (Meaking and Donn 1988).

So far, several works considered the influence of the fractal dust growth on the evolution of protoplanetary disks, but clear consequences have not been established. For example, Weidenschilling et al.(1989) reported that settling to midplane needs much longer time for fractal growth compared with the spherical growth. But later, the result has been shown to be erroneous due to the coarse division in mass coordinates in their numerical code to solve coagulation equation. In addition, fractal dimension of the aggregates in their calculation are not determined in a self-consistent way, but given by an artificial formula.

In order to overcome these problems, detailed analysis of the relavant physical process and mathematical formulation will be made in this paper. Chapter 2 is essentially a continuation of this introduction, reviewing fundamental characteristics of the coagulation in the protoplanetary disk. A new numerical method (Quasi Monte Carlo) to investigate the interaction between fluffy aggregates and gas molecules is presented in Chapter 3. Using this method, we derive a gas drag formulae on the fluffy aggregates in the free-molecule regime. Chapter 4 describes the numerical algorithm to solve Smolchowski's coagulation equation. Further, the interaction between the geometry and the kinetics of the aggregates are explored with Monte Carlo simulations. Finally in chapter 5, the time development of the spatial and size distribution of fractal dust aggregates is examined. The effect on the disk evolution is discussed. Conclusions and future plans are summarized in chapter 6. Some related publications are cited in appendices.

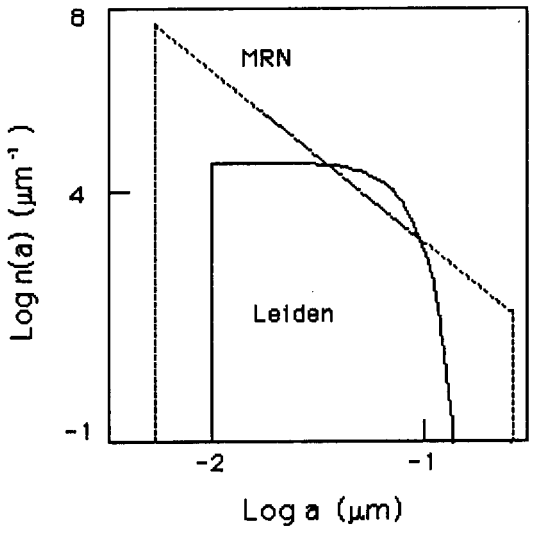

Figure 1:
Size distribution of n(a) for the MRN model and Leiden Model, where n(a) is the number of particles between radius a and a+da. The normalization was done to get unity after an integration of both distributions over a. (Mathis 1988)

2 Fundamentals

Regarding the realistic geometry of the dust aggregates in the protoplanetary disk, the first problem to be considered is the definite size and shape of the constituent particles. In addition, it is preferable to know the chemical composition of the constituent particles for studying the coagulation process because chemical composition can plays an important role on the kinetic aspect of coagulation through sticking probability. These problems will be discussed in the following sections.

2.1 Size and shape of the constituent particles

It is likely that most of the grains in the protoplanetary disk have originated from interstellar dust particles. Then, the size distribution of interstellar dust is a plausible candidate for that of the constituent particles in protoplanetary disks. The study for the size distribution of interstellar dust stands in a controversial area. There are two different types of models for interstellar grains, i.e. Leiden Model (Hong and Greeenberg 1980) and MRN model (Mathis et al. 1977). Both models have been constructed to explain the starlight extinction curve through diffuse interstellar space. Figure 1 shows the size distribution for each model. While MRN model consider spherical dust particles, some elongated geometry is needed to explain the starlight polarization as assumed in Greenberg model. In this paper,however, constituent particles are assumed to be spherical for simplicity.

Naturally, these size distributions in diffuse interstellar space would be considerably altered inside the molecular clouds during a contracting phase by the coagulation and condensation of volatile material on dust grains. Recent works (Rossi et. al. 1991, Ossenkopf 1993) have shown that coagulation driven by thermal motion and cloud turbulence effectively decrease the number of small particles and make the distribution narrower. Thus, we consider the constituent particles of uniform size ($0.1 \sim 1\mu m$) throughout this paper.

2.2 Chemical composition and sticking probability

Two colliding particles can stick together, or bounce or fragment upon collision, depending on their relative velocity, their sizes and their compositions. It is widely accepted that the sticking occurs as

Figure 2:

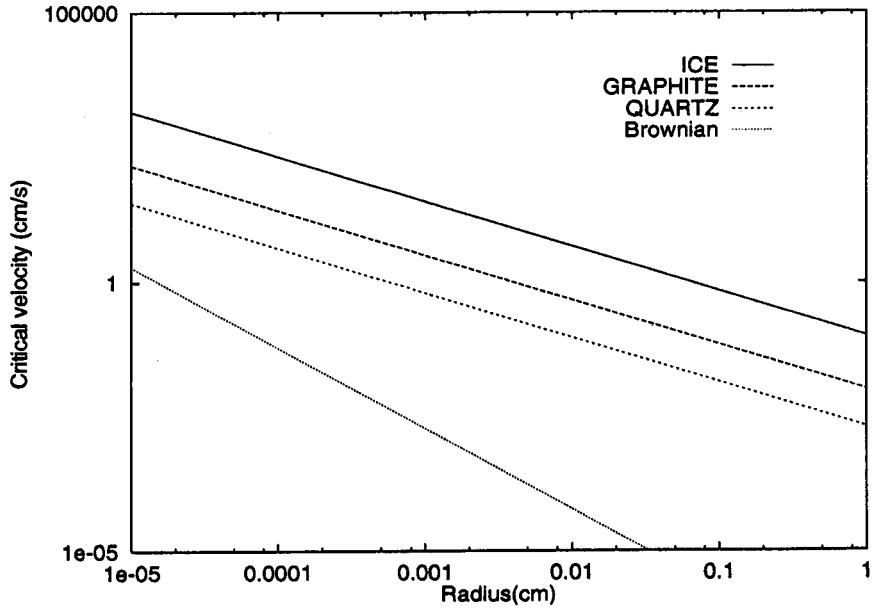

The critical velocity for sticking is indicated as a function of grain radius R for three different materials. The curve labelled Brownian denotes the grain velocity expected due to random thermal motion (Choksi et al. 1993).

a result of low-velocity collision between two small particles. Recently, several attempts to estimate the sticking probability between small particles have been reported (Blum and Munch 1993, Gay and Berne 1986). In this section, we briefly review the theoretical study by Choksi et al (1993).

They derived a critical velocity for sticking as a function of gain size and composition. That is,

$$V_{crtitical} \simeq 3.86 \frac{\gamma^{5/6}}{E^{1/3} R^{5/6} \rho^{1/2}} \tag{1}$$

where R is a radius of colliding particle, E denotes the Young's modulus, ρ and γ , respectively, mean the density and interface energy of the particle. It is obvious from Eq.1 that the smaller particle has larger value of V_{cr} , and the critical velocity also depends on the properties of the particle material. The material with higher interface energy and smaller Young's modulus shows larger critical velocity (see fig.2). It is noteworthy that the velocity due to random thermal motion is always smaller than the critical velocity derived from eq.(1). Therefore, all collisions due to random thermal motion of constituent particles lead to perfect sticking.

The contact between two fluffy aggregates is governed locally by the touching constituent particles, but the kinetic energy by the whole aggregates. Consequently, the critical velocity will scale with $N^{-1/2} \times R^{-5/6}$ where N is the number of constituent particles in the cluster. It implies that PCA has much higher sticking probability than CCA. When the relative velocity exceeds the critical one, the growth enter the stage where the restructuring ,bouncing and fragmentation of the clusters must be taken into account (Meakin and Julien 1988, Donn 1990, Dominik and Tielens 1995). However, we

shall assume perfect sticking throughout this paper.

2.3 Simple models of fractal aggregates

First, the trajectory of the dust particles in the protoplanetary disk is considered. Weidenschiling (1977) derived the formulae to calculate the "reaction time" for a dust particle with mass m and cross section A moving through the ambient gas with the density of ρ_g.

$$t_f = \frac{3m}{4A\rho_g c} \tag{2}$$

where c denotes the sound speed of the gas. With typical physical conditions in a protoplanetary disk, t_f ranges from about 0.1 sec to several hours. Multiplying t_f by the velocity of the particle, we can roughly estimate the length of the inertia motion. A dust particles has a ballistic trajectory if this distance is longer than the size. On the basis of above discussion, we present two fundamental models of collisional coagulation, i.e. BPCA (Ballistic Particle Cluster Aggregation) and BCCA (Ballistic Cluster Cluster Aggregation). BPCA is made by the collisions of a target cluster with single "background" particle. On the other hand, BCCA is a complete hierarchical model where the clusters are formed out of collisions between two clusters having the same number of constituent particles (see Fig.3). An incident cluster (a single particle in case of BPCA) is fired at the target cluster from a random direction with a random impact parameter. The pair is rigidly fixed at their first contact point. We refer to the previous work for the details of their generation processes and the resulting structures(see, e.g. Mukai et al. 1992). BPCA and BCCA corresponds to the extreme growth kinetics, respectively. That is, only a biggest cluster in the system grows in BPCA while only smallest clusters do in BCCA. In the early stage of coagulation, the random thermal motion is dominant. Consequently, smaller clusters with higher mobility are expected to yield quite fluffy aggregates like BCCA (Meakin and Donn 1988). As the growth proceeds, other mechanisms become important through gas-grain interactions. Due to the differences of the gas drag force on the aggregates, settling to midplane of the disk or radial inward drift produce the relative velocity between the different-sized particles. Then, if an aggregate acquires higher relative velocity due to an increase of its mass, the growth rate increases as a result of high relative velocity. What kind of aggregates are resulted from these environments? This problem will be examined in chapter 4 in detail.

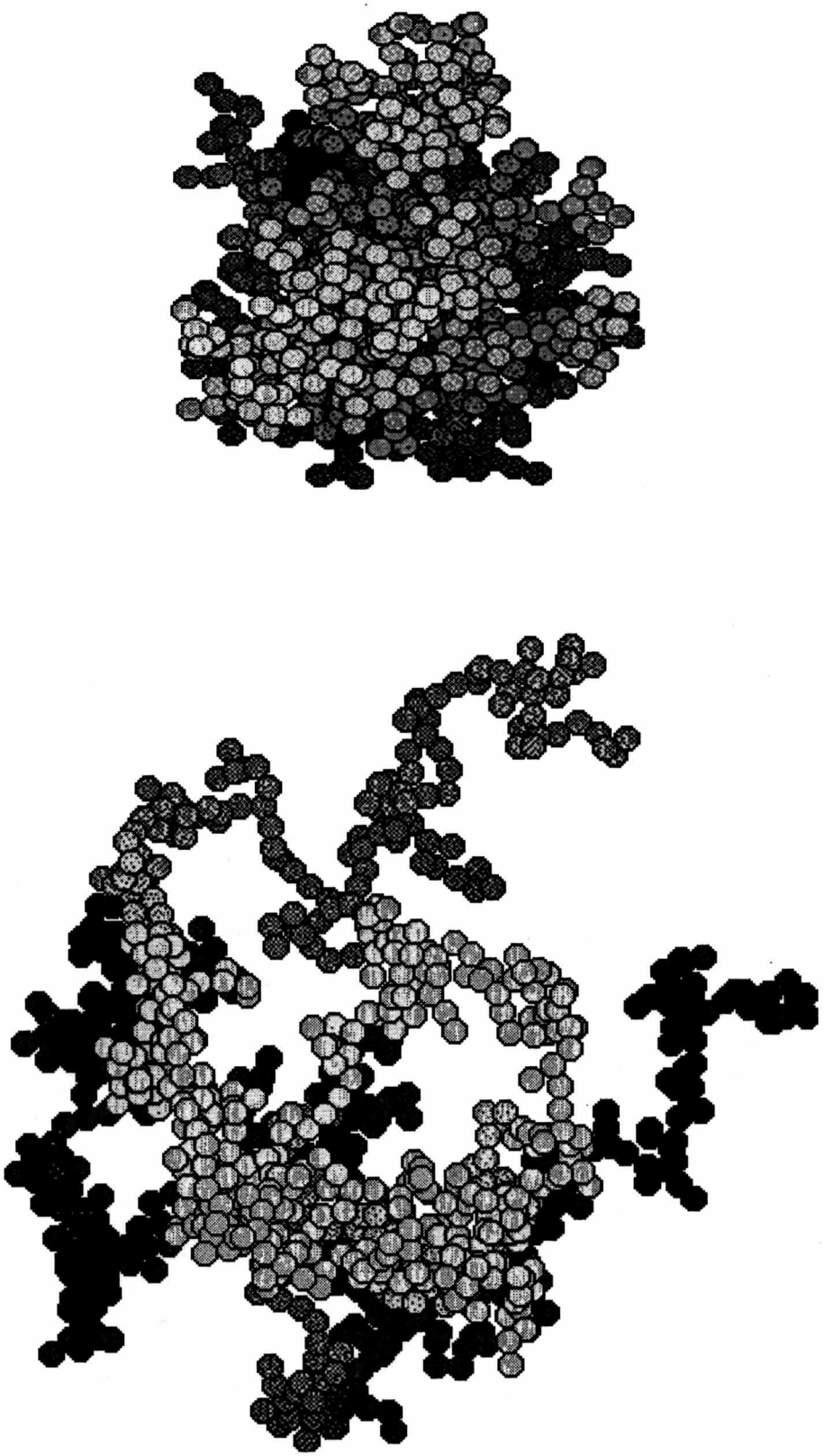

Figure 3: BPCA and BCCA with 1024 constituent particles

3 Free-molecule gas drag on fluffy aggregates

As mentioned in introduction, dynamical behaviour of solid matter is controled by the gas drag force as long as the size is less than kilometer. Therefore, it is indispensable to know the drag force on fluffy aggregates to investigate the early stage of disk evolution. Analytical gas drag formulae in the free molecule region, available only for some simple shape with convex geometry (Dahneke 1973), yield a well known result that the drag force is proportional to the projected area of the target. Thus, most of previous literatures (e.g. Weidenschilling and Cuzzi 1993) have simply assumed that the drag force on fluffy aggregate is proportional to the projected area as well. The verification of this intuitive conjecture is the main issue in this section. Also, we frequently encounter the astrophysical situation where the mean free path of the gas molecules is comparable to the size of an aggregate and the relative velocity between the dust and the gas is much smaller than the mean thermal velocity of the gas. For a spherical particle having the diameter D and the relative velocity U to the surrounding gas, the drag force F in the transition regime is expressed by (e.g. Ying & Peters 1991)

$$F = \frac{3\pi\eta DU}{C(D)} \tag{3}$$

$$C(D) = 1 + Kn[\alpha + \beta exp(-\gamma/Kn](Kn = \lambda/D) \tag{4}$$

where λ is the mean free path and η is the viscosity of the gas. Although the values for the quantities α, β and γ have been determined mainly from experiments (Table 1), Takata et al.(1993) has given theoretical basis of this formula, solving Boltzmann equation numerically.

Dahneke (1973) proposed "adjusted sphere" generalization of eq.(4) for nonspherical particles. In spite of its simplicity, the interpolation method has been proved to satisfactorily predict the drag force on plate(Chen et al. 1988) , cylinders or chains (Pich 1969). In order to recover the correct limiting behavior, eq.(4) is modified as follows.

$$F = \frac{3\pi\eta D_{\rm m} U k_{\rm c}}{C(D_{\rm a})} \tag{5}$$

where $D_{\rm m}$ denotes the diameter of the sphere of same mass as the nonspherical particle and $k_{\rm c}$ is the dynamic shape factor in continuum regime defined as the ratio of the drag forces between the aggregates and a sphere having the same mass and velocity. Moreover, $D_{\rm a}$ is "adjusted diameter" of an adjusted sphere whose free-molecule limit of $C(D_{\rm a})$ is equal to that of the specified nonspherical particle. In short, the formula provides the smooth connection over the intermediate Kn range with reproducing correct limiting behavior (Rogak et al. 1993). While the values of $k_{\rm c}$ for fractal aggregates have been obtained in numerous works (see e.g., Rogak and Flagan 1992), the number of studies for

Table 1:
Coefficients for slip correction factor

Author	α	β	γ
Seinfeld (1986)	1.257	0.4	1.1
Allen and Raabe (1985)	1.142	0.558	0.999
Hutchins et al. (1995)	1.2310 $\pm$ 0.0022	0.4695 $\pm$ 0.0037	1.1783 $\pm$ 0.0091

free molecular drag is rather limited.

Meakin et al. (1989) investigated the drag force on fractal aggregates in Epstein regime where a relative velocity of aggregate to the ambient gas is much smaller than the mean thermal velocity of the gas. On the other hand, our previous work (Nakamura et al. 1994) treated the aggregate moving much faster than the mean thermal velocity. Both are based on the assumption that the gas drag force can be expressed as the product of following two independent factors, i.e.,

- the number of molecular collisions per unit time
- the mean momentum transfer per collision

While the former is supposed to be proportional to the relative velocity and the projected area of the aggregate, the latter depends on the surface structure of the aggregate and also the model for the molecular-particle interaction. It is difficult to estimate these factors for fluffy aggregates because

- a certain fraction of the surface of the aggregate is shielded from the impinging molecules
- a molecule may experience multiple reflection on the surface

Since these effects make an analytical evaluation infeasible, the previous researchers resorted to Monte-Carlo simulations. They made independent estimate of the two factors and simply combined them, neglecting a possible correlation between them. Although each result quantitatively confirmed the conjecture that the gas drag force on fractal aggregates can be estimated by that on a sphere of equivalent geometrical cross section, the validity of the basic assumption that the drag force can be separated into two factors is still an open question. Another important restriction of these works is the extreme range of the relative velocity between the gas and the aggregate. Naturally, the gas drag formula, which can be applied to whole range of the relative velocity, is strongly desired.

We present a new model to simulate the relevant physical processes as similar as possible in the numerical scheme. It involves the concurrent evaluation of the rate of molecular collisions on a surface element and the resulting momentum transfer by one collision and covers the entire range of the relative velocity to the gas.

3.1 Computational procedures

First, the velocity distribution of gas molecules is assumed to be Maxwell-Boltzmann distribution at a virtual sphere enclosing the target aggregate. Since we concern a free molecular limit here, the presence of the aggregate does not modify the velocity distribution of molecules. Next, we make the assumption how an incident molecule is reflected at the surface of the aggregate. Meakin et al. (1989) have investigated three cases of reflection, i.e., specular collisions, cosine law diffuse collisions and random diffuse collisions. In this section, only specular reflection model is considered for simplicity. But, extension of the model to treat other reflection models is rather straightforward.

Based on the above assumptions, the drag force is estimated by the following procedure. We take a Cartesian coordinate system moving together with the target aggregate. During the collision, the origin of the coordinate is fixed at the center of mass of the aggregate since the mass of the target aggregate is much larger than that of an incident molecule. Incident molecules are successively fired

to the virtual sphere enclosing the target aggregate. Taking into account multiple reflections of a gas molecule on the rough surface of the aggregate, we follow the trajectories of incident gas molecules. Since all reflections are supposed to be specular, the momentum transfer can be calculated for each collision.

The contribution of one molecule to the drag force is estimated by calculating f, the momentum variation of an incident molecule along the moving direction of aggregate multiplied by the relative velocity. Total drag force is obtained by taking E_N, the arithmetic mean of f

$$E_N = \frac{1}{N} \sum_{k=1}^{N} f(\vec{x_k}) \tag{6}$$

where N is the number of incident molecules. In order to specify one incident molecule, we need five variables, i.e., two coordinates for the impact parameter and three velocity components of the incident gas molecule. The latter components are given by the summation of the velocity of the aggregate with respect to the coordinate system and the velocity of the molecule in coordinate system. This procedure corresponds to multivariate integration of an irregular function. Next problem is how to pick up efficient sampling points ($\vec{x_k}$ sequence), i.e., specify the velocity and impact parameter of an incident molecule to evaluate the integrand. We will pursue this problem in the following subsection.

3.2 Search for optimal sampling points

It is widely known that Monte Carlo method with standard pseudo-random sequences (MC) has a great advantage in multivariate integration of complex functions compared with standard numerical integration methods, such as a trapezoidal rule. The merit is mainly derived from the property that the error bound for MC is independent of the dimension of the integrand while the error bound for standard procedures increases exponentially with the dimension. However, the error bound for MC is not upper limit. We must be content with weaker guarantee that the error is probably no more than $\sigma/\sqrt{N}$. Here σ is the variance of the result and N denotes the number of sampling points (Traub and Wazniakowski 1994). Popularity of MC doesn't mean that it is optimal selection. In practice, the rate of convergence of MC is rather slow. Theorem of large number indicates that the accuracy increases only as the square root of N.

Alternatively, the Quasi Monte Carlo method (QMC) has been proposed as an efficient method to calculate the multivariate integration (Niederreider 1978). Instead of ordinary pseudo random sequences, QMC adopt quasi-random sequences as sampling points. Quasi random sequences generate the sample points "maximally avoiding" of each other for efficient uniform sampling of n-dimensional space. It should be noted that the term "random" is somewhat misnomer since they are produced in a perfect deterministic way. Several previous works (Sarkar & Prasad 1987 ; Bratley & Fox 1988) have shown QMC gives much faster convergence than MC. In addition, QMC has a rigorous error bound if the integrands are functions of bounded variation in the sense of Hardy and Klause (Niederreider 1978). Unfortunately, this estimation of the error bound is irrelevant to our case because the scattering functions of incident molecules are not of bounded variation. Then, a practical way is necessary to sidestep the intricate estimate of the error bound even with QMC. Following Fox(1986), we check the stability of the temporal estimate E_N. A calculation is terminated when the estimated relative error $|E_{2N} - E_N|/E_{2N}$ becomes less than a certain tolerance (we call it "convergence criterion") and N is larger than a certain threshold. To avoid an accidental false convergence, we also check

$|E_{2N} - E_{N/2}|/E_{2N}$. Obviously, this procedure still leaves some uncertainty about the accuracy, but that is unavoidable.Among several variations of QMC (Fox 1986), we have employed an improved Sobol's method implemented by Press et al.(1991) because it turned out to be most efficient and accurate in most applications including numerical multivariate integration.

3.3 Comparisons of the rate of convergence

We begin with the comparison of the results of our numerical calculations with an exact analytical formula for a sphere. In the case of specular reflection, the gas drag force F_D on a spherical particle with a radius a is given by $F_D = 2C_D\pi a^2\rho U^2$ (Baines et al. 1965). Here, U is a relative velocity of the grain to the gas, ρ denotes mass density of the gas and C_D is a drag coefficient defined as

$$\frac{1}{2\sqrt{\pi}}\{ (\frac{1}{S} + \frac{1}{2S^3}) \exp\left(-S^2\right) + (1 + \frac{1}{S^2} - \frac{1}{4S^4}) \sqrt{\pi}\mathrm{erf}(S) \} \tag{7}$$

where S is a ratio of the relative velocity U to the mean thermal velocity of the gas v. This rather complicated expression can be simplified for two limiting cases. When S >>1, the drag coefficient approaches 2 and F_D is proportional to the square of the relative velocity. On the other hand, when S <<1, the well-known Epstein law is obtained, i.e., $F_D = (4\pi/3)a^2\rho vU$.

Figure 4 shows the results for S = 1, where the absolute values of fractional accuracy are plotted as a function of N, the number of incident molecules. The values are averaged for 10 trials. Although QMC gives completely deterministic sample points as mentioned in the preceding subsection, we can realize different trials with changing assignation of an identical sequence to five variables. Fractional accuracy for MC shows $N^{-1/2}$ asymptotics as expected. One can easily find that QMC substantially outperform MC with much more rapid convergence. For example, when the estimate of the drag force with 0.1 percent accuracy is required, QMC meets this condition with only a few ten thousands points ,whereas MC requires more than million points. The ratio would be even greater for higher accuracies.

Subsequently, the rate of convergence for irregularly shaped aggregates is investigated. Since no analytical solution is available for this case, we must rely on the temporal estimation of relative error defined in the previous subsection. Figure 5 shows the development of the averaged relative error for the case of BPCA with eight particles. It should be noted that one can see no distinct differences in the structure between BPCA and BCCA at this size. Although the difference is not so significant for the case of sphere, we can see QMC converges faster about one order of magnitude if 0.1 percent accuracy is required. It can be concluded from these examples that our model with QMC outperforms ordinary Monte-Carlo with pseudo-random sequences and provides reliable estimate of the drag force with moderate computational costs. Therefore, we adopt QMC for all the calculations in the following subsections.

3.4 Results

In contrast to the case of a sphere, the fluffy aggregates have large anisotropy in their shape. Thus, two directions of the motion are selected to represent extreme cases. One is the direction along the axis with maximum momentum of inertia of the aggregate (X direction), and another is that for minimum (Z direction). Roughly speaking, these directions give the biggest and smallest projected area of the aggregate, respectively. Since the aggregate contains large amount of vacuum, many molecules fired to the virtual sphere enclosing the aggregate miss the target. Figure 6 shows the collision probability, i.e.

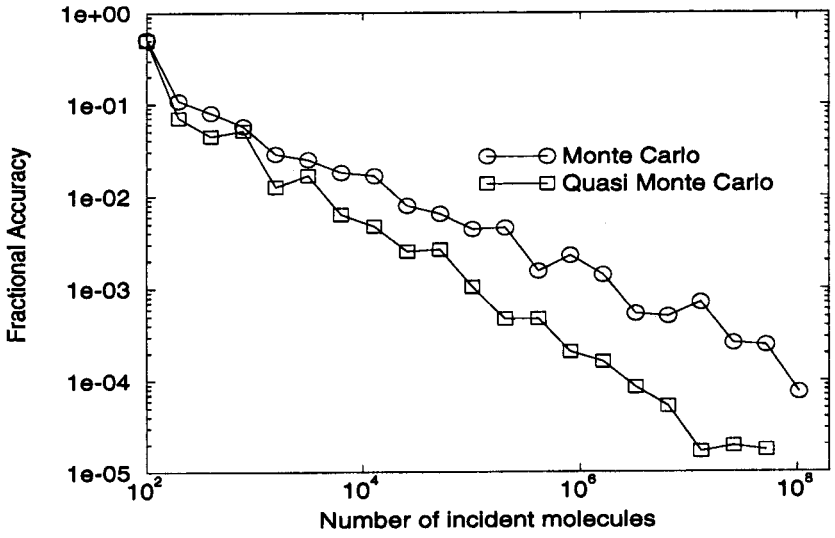

Figure 4:
Fractional accuracy of numerical calculations to an exact analytical value. The target is a sphere moving with S = 1.

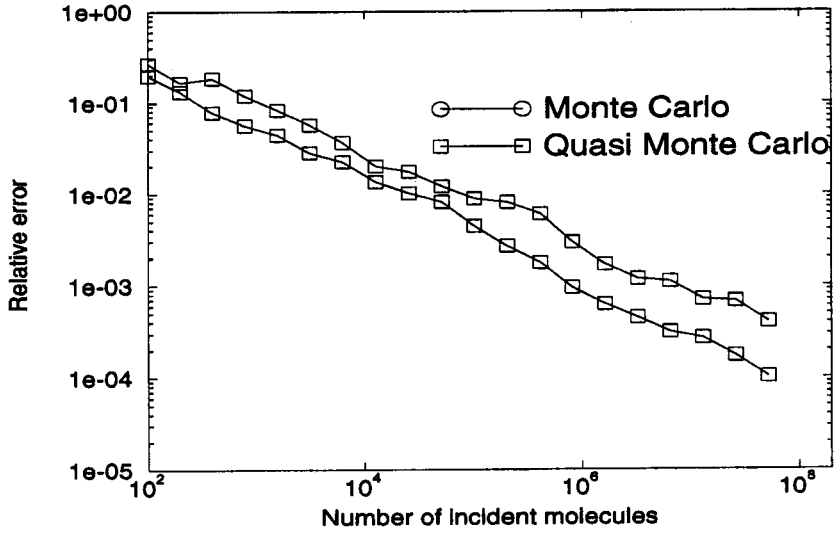

Figure 5:
Temporal relative error vs number of incident molecules average for 10 different trials. The targets are BPCA with 8 constituent particles moving with S=1.

the fraction of impinging molecules which experienced at least one collision. The targets are BPCA with 8 constituent particles and two-touching spheres. While the fraction is not dependent on moving direction when S << 1, anisotropy becomes clear as S increases. For two-touching spheres, two representative directions correspond to the perpendicular motion, in which it translates orthogonally to its line of centers, and the parallel motion along its line of centers, respectively. Moreover, the radius of the enclosing sphere is twice as that for a constituent sphere. Consequently, collisional probability becomes 0.5 for X direction and 0.25 for Z direction in high velocity limit.

The product of this collision probability and the surface area of an virtual sphere enclosing the target aggregate can be interpreted as surface area of the target when S << 1. Further, this quantity completely agrees with the projected area of the target measured by Meakin and Donn (1988) and Ossenkopf (1993) as the molecular motion approaches one way flow with S increasing. In other words, "surface/projected area equivalent sphere" can be defined so that the sphere moving with same velocity experience the same number of collision of molecules as the fluffy aggregates. If the collision probability in high velocity limit is averaged for three directions, it is nearly same to that for S<< 1. If we adopt this 'mean' collision probability globally, however, the resulting drag forces reflect the variation of the collision probability depending on the moving direction. In order to eliminate this effect, the local collision probability at a certain value of S is adopted to determine 'adjusted sphere diameter'.

In fig. 7, the ratios of drag force on tow-touching spheres and BCCA to that on area-equivalent sphere are indicated. Setting convergence criterion as 1 %, we took an average for ten aggregates for each size. Strictly speaking, the ratio differs from "mean momentum transfer" defined in our previous work. Yet, we can find the similarity between them as the efficiency of momentum transfer normalized by that for a sphere. It should be emphasized that the ratio indicates anticorrelation with the collision probability. As a result of this cancelation , the variation of the drag force ratio becomes less distinct if the actual drag is globally normalized by the collision probability for S<<1. It has been revealed that the ratio depends on the size and the structure of the aggregate, but less than 25 % for entire range of S. Further, one can see that the drag force differs by 30% even when $S << 1$, though collision probability is nearly same. Hence, the actual drag force depends on the moving direction not only for $S >> 1$ where the shape anisotropy appears, but for $S << 1$. What is the reason of this variation of the drag force ratio? Naturally it is expected that the process irrelevant for spherical target is responsible for this variation. In order to confirm this, the distribution of f for two-touching spheres is indicated in figs. 8 and 9. Note that we set the mass of an incident molecule and the mean thermal velocity to be unity. While the distribution for molecules with only one collision is indistinguishable from that for sphere, the distributions for molecules with multiple reflection is altered remarkably. When the two-touching spheres are moving in X direction, fraction of "back-scattered" molecules with positive value of f becomes larger compared with the sphere. On the other hand, it becomes smaller for Z direction as shown in fig.9.

In their pioneering work, Chan and Dahneke (1981) investigated the free-molecule drag on two-touching spheres. Multiplying the momentum transfer for each collision by the molecular collision rate on a surface element and taking the sum over the entire surface, they obtained the drag force in a wide range of the relative velocity. Since they have integrated a molecular collision rate in advance and neglected the influence of screening by adjacent sphere on total collision rate, the correlation effect is not considered in a rigorous manner. Nontheless, our calculations show an fair good agreement with their results. Table 2 exhibits the ratios of the drag force on two-touching spheres to that on single constituent sphere in the case of S = 0.1 where the difference between the exact formula (5) and

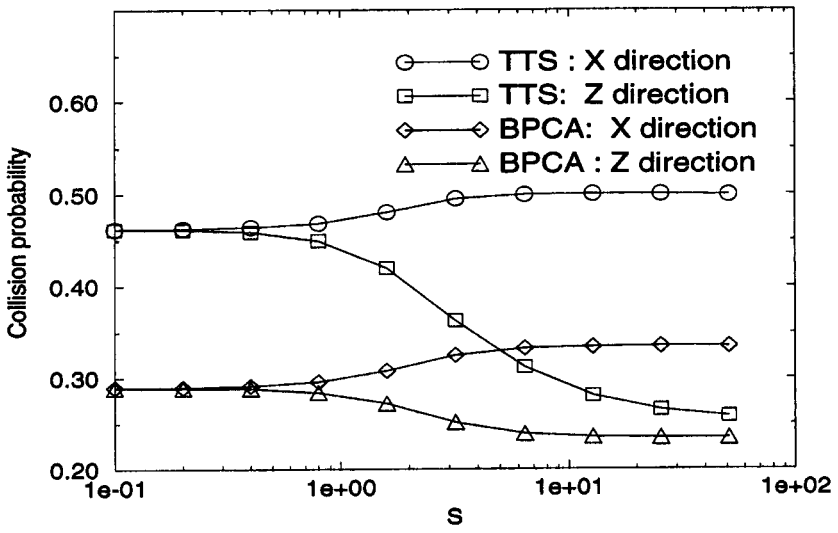

Figure 6:
Fraction of incident molecules experienced at least one collision . The horizontal axis represents S, the velocity of the aggregates normalized by mean thermal velocity of the gas. The targets are two-touching spheres(TTS) and BPCA with 8 constituent particles.

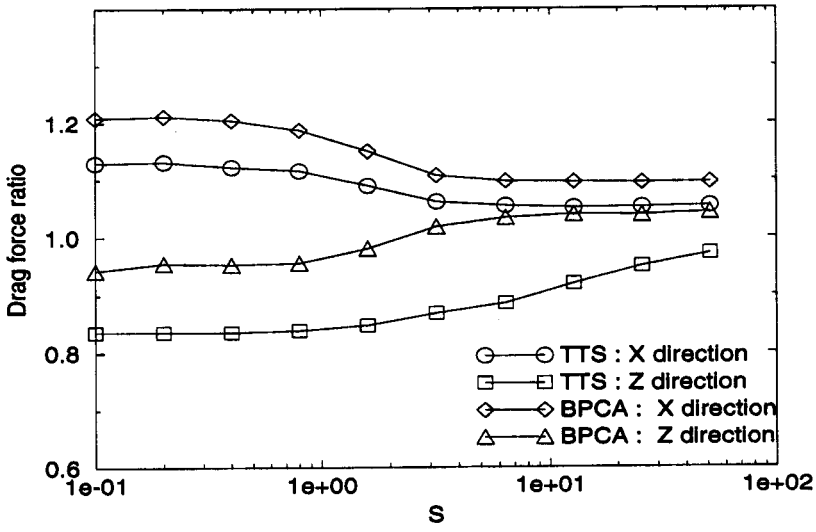

Figure 7:
The ratios of actual drag force on the target to that for "area equivalent sphere".

Table 2:
A ratio of the drag force on two-touching spheres to that on single sphere

Author	Parallel	Perpendicular
Chan and Dahneke	1.5478 ± 0.0047	2.08623 ± 0.00716
Present work	1.54397 ± 0.00057	2.09002 ± 0.00043

Epstein law is less than 1 %. Total number of impinged molecules is 52 428 800 and averaged values for 5 trials were taken.

Figures (10) – (13) show the dependence of the drag force ratio on S for the fractal aggregates. A huge number of incoming molecules is necessary even with QMC as S decreases or the structure of the target becomes fluffier because the absolute value of the drag force becomes quite small in such cases. It is apparent that the ratio considerably changes around $S \sim 1$ in any cases. For BPCA, the values for high velocity asymptotic seem to increase with the size for both directions. In contrast, curves for BCCA approach a same limiting value, i.e., 8 % enhancement, regardless of the size and the moving direction. On the other hand, one can see no evident trend in the low velocity limit. For Z direction, the low velocity asymptotic values increases with size for both types of the aggregates, whereas the values for X direction remain about 16% enhancement for BPCA and decrease slightly for BCCA if the aggregate has more than 128 constituent particles.

We have previously reported the 'mean momentum transfer', the averaged efficiency of momentum transfer per collision compared with a sphere, is larger by approximately 10 % for BCCA and 20 % for BPCA in the high velocity limit (Nakamura et al. 1994). Although we have employed the aggregates of same size for both simulations, drag force ratio for BPCA and BCCA in a large S limit for present calculations is around 11 %, and 8 %,respectively. This discrepancy can be understood as the manifestaion of a correlation between the mean momentum transfer and the collision rate which has not been considered in our previous work.

Further, we can compare our results with the estimation by Meakin et al.(1989). They used more refined models than BCCA to generate the cluster-cluster aggregates. Moreover, they investigated several different models of the interaction between the aggregate and the molecules for $S < 1$. They found that the drag force ratio of cluster-cluster aggregates containing more than several hundreds constituent particles is larger by 9 % for the specular reflection model. In this case, another possibility arises for this discrepancy, namely, the difference in the structure of the target. At present, it seems impossible to distinguish these two possibilities. Ossenkopf (1993) has shown that the ratio of the projected area to the mass for BPCA and BCCA is much greater than that for mass-equivalent sphere. Taking into account his results, we can deduce that the drag force on fluffy aggregate is much larger than that for mass-equivalent sphere. The enhancement mainly comes from the increase of projected area.

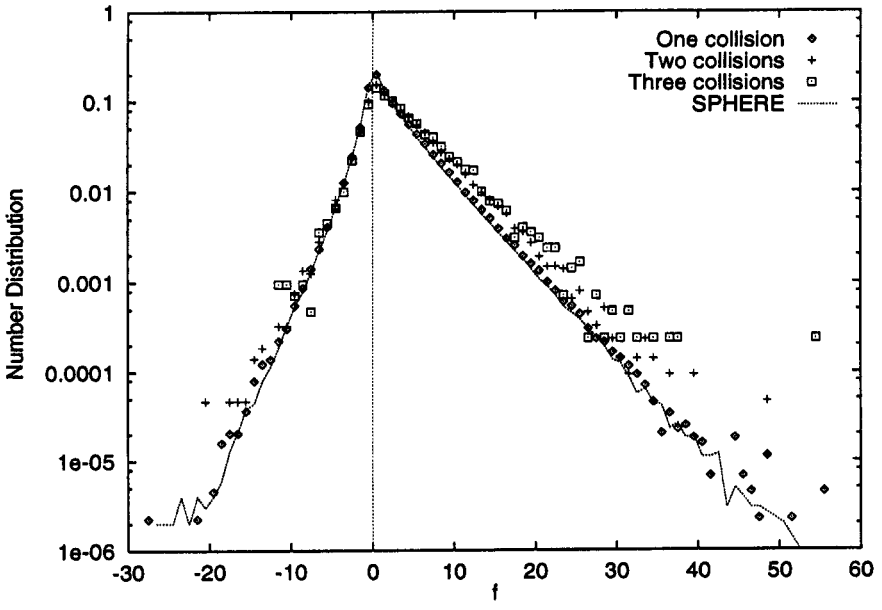

Figure 8:
The distribution of f, momentum variation multiplied by the incident velocity. The target is two-touching spheres moving in X direction with S = 1

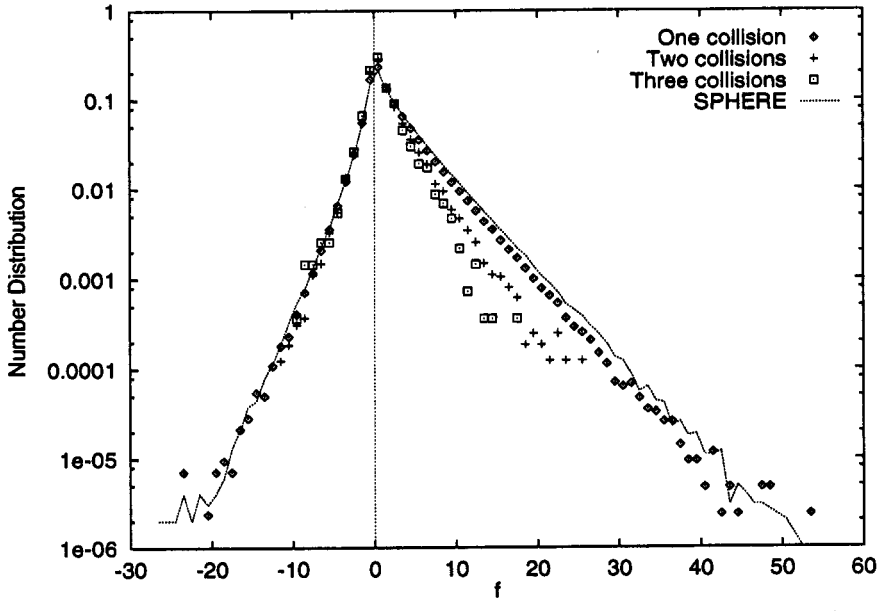

Figure 9:
Same as fig.8, but for Z direction

Figure 10:

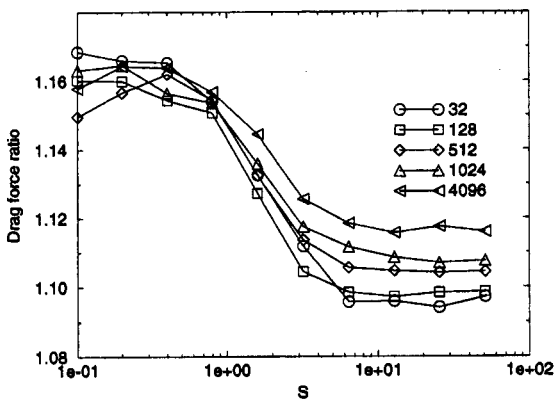

Drag force ratio of BPCA moving in X direction to area-equivalent sphere . Convergence criterion is 1%. For every size, an average for ten different aggregates is taken.

Figure 11:

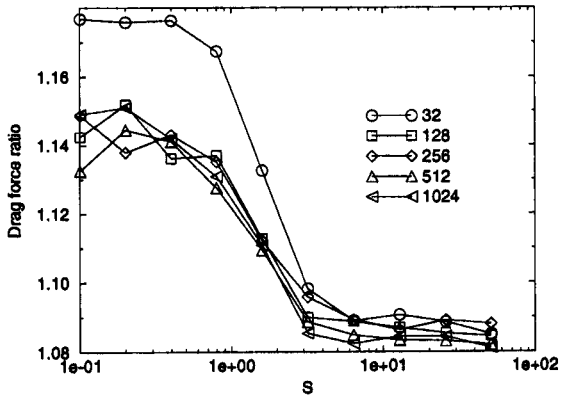

Same as fig.(10), but for BCCA

Figure 12:

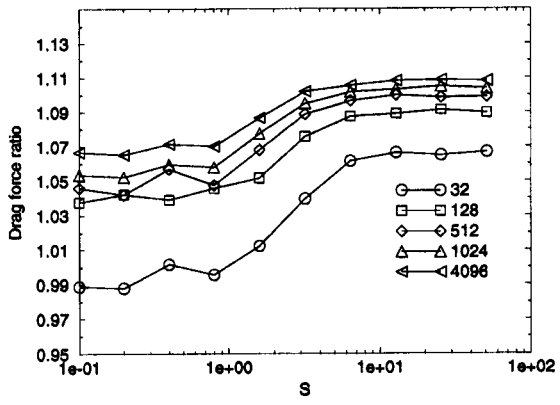

Same as fig.(10), but for the motion in Z direction

Figure 13:

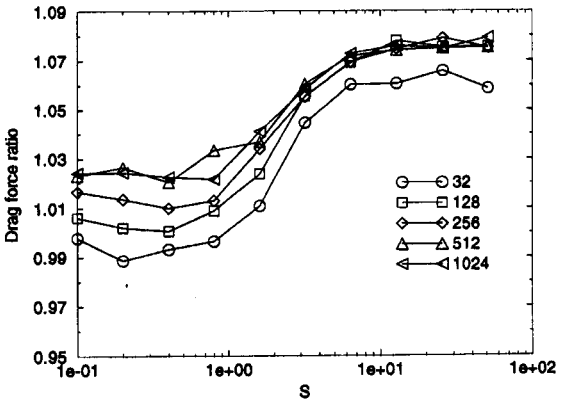

Same as fig.(12), but for BCCA

4 Coagulation Equation

Smoluchowski's "Coagulation Equation" has been widely adopted to describe the evolution of the dust particle or planetesimal size distribution. That is

$$\frac{\partial}{\partial t}n(m,t) = \frac{1}{2}\int_o^m K_{m-m',m'}n(m',t)dm' - \int_0^\infty K_{m,m'}n(m,t)n(m',t)dm \tag{8}$$

or in discrete form as

$$\frac{dn_k}{dt} = \sum_{i+j=k} K_{ij}n_i n_j - n_k \sum_{i=1}^{\infty} K_{ki}n_i \tag{9}$$

Here n_k denotes the number density of k-mer (the particle with mass k) and K_{ij} is the collision rate between i-mer and j-mer. In these equations, the fragmentation resulted from high velocity collisions is neglected. In addition , sticking efficiency is assumed to be unity independent of the size of the dust aggregates as noted in chapter 2. Although this deterministic approach, represented by a set of differential equations, is quite popular, the limitation should be understood correctly. This fomulation involves two important appproximations, i.e., the mean-field assumption and the lowest order clusure. (see, e.g., Sampson and Ramkrishna 1985,1986). A following section will investigate these problems in detail.

4.1 Validity of coagulation equation

From the end of 1960's to the beginning of 1970's, the validity of coagulation equation as a model for droplet coalescence in a warm cloud has occasioned a lively debate in the field of atmospheric sciences (Prupaccher and Klett 1978). Some authors claimed the equation is stochastically incomplete because it describe only the average behavior and the fluctuation is neglected. Probably, most important contribution to this problem was the paper Bayewitz et al (1974). They employed more fundamental description of a random coagulation process with M monomers in a finite system. The so-called Master equation is formulated as

$$\dot{P}(\mathbf{m},\mathbf{t}) = \frac{\mathbf{1}}{\mathbf{2M}} \sum_{\mathbf{(i,j)}} \mathbf{K_{ij}P(m_{ij}^{+},t)(m_i+1)(m_j+1-\delta_{ij})} - \mathbf{P(m,t)\ m_i\ (m_j - \delta_{ij})} \tag{10}$$

Here, $\mathbf{m} = \{m_l\}$ represents a cluster distribution: m_1 monomers,m_2 dimers,m_3 trimers,$\cdots$ etc. $\mathbf{m}_{ij}^{+} = \{m_l + \delta_{il} + \delta_{jl} - \delta_{i+j,\,l}\}$ represents a similar distribution containing an extra i-mer and j-mer and one less (i+j)-mer. $P(\mathbf{m},\mathbf{t})$ is the probability that the cluster distribution at time t is $\mathbf{m}$. For monodisperse intimal conditions,

$$\begin{aligned} P(\mathbf{m},\mathbf{t}) &= 1, \quad if \quad \mathbf{m} = \{\mathbf{M},\mathbf{0},\mathbf{0},...,\} \\ &= 0, \quad otherwise \end{aligned} \tag{11}$$

While coagulation equation (9) gives a deterministic description, Master equation provides a more realistic picture of stochastic coagulation processes with intrinsic fluctuations. Many authors have proved that coagulation equation derives physical validity as the limit of this equation (Tanaka and Nakazawa 1994, Lushnikov 1978, Hendriks et al. 1985) Here, we overview the proof following Spouge

(1985).

The generating function of $P(\mathbf{m}, \mathbf{t})$,

$$\psi(\mathbf{x}, \mathbf{t}) = \sum_{(\mathbf{m})} \mathbf{P}(\mathbf{m}, \mathbf{t}) \mathbf{x_1}^{\mathbf{m_1}} \mathbf{x_2}^{\mathbf{m_2}}, \cdots \mathbf{x_m}^{\mathbf{m_M}} \tag{12}$$

satisfies

$$M \frac{\partial \psi}{\partial t} = \frac{1}{2} \sum_{(i,j)} K_{ij} (x_{i+j} - x_i x_j) \frac{\partial^2 \psi}{\partial x_i \partial x_j} \tag{13}$$

Applying the operator $x_l \frac{\partial}{\partial x_l}$ to Eq.(13) and evaluating the result at $x_1 = x_2 = x_3 = \cdots = x_m = 1$ yields

$$M \frac{d\overline{m_k}}{dt} = \frac{1}{2} \sum_{i+j=k} K_{ij} (\overline{m_i m_j} - \overline{m_i} \delta_{ij}) \; - \sum_{i\,=\,1}^{M} K_{ik} (\overline{m_i m_k} - \overline{m_i} \delta_{ik}) \tag{14}$$

where the upper bar means an expectation. Iterating this procedure, one can generally indicate that the evolution of N-order correlation will include N+1-order correlation. To terminate this infinite expansion, a closure hypothesis, a relation between N and N+1 correlation, is needed (Sampson and Ramkrishna 1986). Coagulation equation is derived from the lowest order closure:

$$cov(\frac{m_k}{M}, \frac{m_l}{M}) \; = \; \frac{1}{M^2} (\overline{m_k m_l} - \overline{m_k} \; \overline{m_l}) \; \rightarrow \; 0 \qquad as \;\; M \rightarrow \; \infty \tag{15}$$

Setting $N_k = \overline{m_k}/M$, one can easily confirm that Master equation (10) becomes equivalent to Coagulation equation. From eq.(15), it can be concluded straightforwardly that coagulation equation neglects the correlations and fluctuations of cluster number in a real system. Consequently, its utility must be severely constrained when the fluctuation play an important role for the evolution of the system. From this point of view, the system size should be set as large as possible.

Up to now, only special types of kernels are known to have analytical solutions (see table 3). They are constant kernel, kernel proportional to the sum of the two colliding mass, and kernel proportional to the product. The exact solutions for monodisperse initial condition are summarized in table 3. Derivations using generating function method can be found in the appendices of a series of papers by van Dongen (1987 II,III). Similarly, their stochastic counterpart have been also obtained. (see e.g. Hendriks et al. 1985). Tanaka and Nakazawa (1994) examined the condition under which the solutions of Master equations are reduced to that for corresponding coagulation equation. While they considered not equation itself, but the solution, van Dongen and Ernst (1987 II) investigated the validity criteria for coagulation equation with such exactly solvable kernels using van Kampen's Ω-expansion method. Both authors found that coagulation equation with the product kernel is valid only if the mean cluster size $S \ll M^{2/3}$. van Dongen (1987 III) extended the study and obtained a general condition for non-gelling homogeneous kernels, i.e., $S \ll M$. The case for constant kernel has been studied with various methods, such as direct spatial simulation (Mulholland and Mountain 1986), higher order closure hypothesis (Murthy 1987) or analytic solutions of Master equation (Bayewitz 1974).

Another problem in the formulation of coagulation equation is the absence of spatial information. Namely, it is based on mean-filed assumption that particles are uniformly distributed independent of

Table 3:

Kernel	f	N_k
Constant	$(1+t/2)^{-1}$	$f^2(1-f)^{k-1}$
Sum	$\exp(-t)$	$\frac{k^{k-1}}{k!}f(1-f)^{k-1}\exp(-k(1-f))$
Product	$1-t/2$	$\frac{(2k)^{k-1}}{k!k}(\frac{t}{2})^{(k-1)}\exp(-kt)$

Exact solutions for monodisperse initial condition. Total mass and the time t in the system are normalized to be unity. f and N_k denotes the total cluster number and fraction of k-mer, respectively.

the location in the system. As particles in a given region undergo a series of coagulation, however, there is a corresponding decrease in the number of particles in that region available for further coagulation.If the diffusion is not rapid enough to compensate this effect, correlations between particle numbers and the spatial inhomogeneity is not completely washed out. Hence, mean-field assumption is justified only when the time scale for coagulation is much longer than diffusion time scale (Nicolis and Prigogine 1989). Actually, diffusion-limited systems have an upper critical dimension under which mean-filed assumption breaks (Ziff et al. 1985, Kang and Redner 1984). Most well-known example is the dynamical befavour of one dimensional models, such as diffusion-reaction model (Doering 1990) and ballistic aggregation model (Jian and Leyvaz 1993,1994),. Since settling induced coagulation in the protoplanetary disk is expected to be one-dimensional process, we should pay a special attention to this problem. Wright et al. (1993) and van Dongen (1989) should be referred for recent progress. In order to account for the spatial inhomogneity, an diffusion or transport term, such as $\partial n_k v_k/\partial z$, can be added to coagulation euqation. However, this approach becomes inconsistent with mean-field assumption if the spatial gradient becomes so steep. For example, Nakagawa et al. (1981) and Ohtsuki and Nakagawa (1988) logarithmically divide the spatial coordinate to give higher resolution near the location of concern. It means this approach requires a prediction about resulting spatial homogeneity in advance. However, the consistency of the ansatz have not been checked. And even if the ansatz is correct, it cannot exclude other completely different distribution.

In this section, the physical and mathematical basis of coagulation equation have been investigated. The system size should be as large as possible, in order that the effect of fluctuations is small (see eq. 15). In contrast, the smaller system size is preferred for the mean-filed assumption. Further, homogeneity of the physical parameters affecting the collision kernel impose the upper limit of the system size. Consequently, we should choose the system size very carefully to fulfill these two contradictory conditions. This will be the main subject in section 5.4.

4.2 Scaling properties

We begin with the introduction of moments $M_n(t)$ of the size distribution, which is an quite important tool in our argument.

$$M_n = \sum_{k=1}^{\infty} k^n N_k \tag{16}$$

Thus, the zeroth moment M_0 is the total cluster number and the first moment M_1 should be constant if the mass in a system is conserved. Most of previous analytical studies on coagulation equation is

based on two major assumptions, namely the kernel homogeneity and the scaling property of the size distribution. The first assumption is represented by

$$K_{ai,aj} \propto \mathrm{a}^{\lambda}\mathrm{Kij} \tag{17}$$

$$K_{ij} \sim i^{\mu} j^{\nu} \quad (\mathrm{j} \gg \mathrm{i},\ \lambda = \mu + \nu) \tag{18}$$

Moreover, the cluster size distribution normalized by "mean cluster mass" $S(t)$ is assumed to tend towards an invariant form Φ

$$N_k = \frac{M_0}{S^2(t)} \Phi\left(\frac{k}{S(t)}\right) \tag{19}$$

Substituting eqs.(17) and (19) in eq.(9), we obtain two important equations connected with separation constant w, i.e.,

$$-w[x\Phi'(x) + 2\Phi(x)] = \lim_{\varepsilon \downarrow 0} \frac{1}{2} \int_{\varepsilon x}^{(1-\varepsilon)x} dy\ K(y, x-y)\Phi(y)\Phi(x-y) - \Phi(x) \int_{\varepsilon x}^{\infty} dy\ K(x,y)\Phi(y) \tag{20}$$

$$\frac{dS(t)}{dt} = wS^{\lambda} \tag{21}$$

While the former determines the static shape of the scaling function, the latter describe the evolution of "mean cluster size". Equation (20) has the following invariance properties. Let $\Phi(x)$ be the solution of eq.(20) for some constant w. Then for all $a, b > 0$,

$$\overline{\Phi}(\overline{x}) = b\Phi(\overline{x}/a) \tag{22}$$

also satisfies eq.(20) with

$$\overline{w} = ba^{1+\lambda} w \tag{23}$$

Thus, their exists a two-parameter family of scaling function which determines the scale in x and Φ axis. To determine the values of parameters a and b, two conditions must be imposed. For non-gelling systems, the first condition is the mass conservation . In terms of scaling function, that is

$$p_1 = \int_0^{\infty} x\Phi(x)dx = \text{constant} \tag{24}$$

Throughout this paper, we set $p_1 = 1$. A second condition is given by a precise definition of the mean mass S. Different definitions corresponds to different values of a and b. Conventionally, S is defined as the ratio of consecutive moments, i.e.,

$$S(t) = M_2/M_1 \quad or \quad M_1/M_0 \tag{25}$$

Using these rather simple formed kernel characterized by the exponents μ, ν and λ and the scaling assumption, the kinetics of coagulation processes can be described quantitatively (van Dongen and Ernst 1985 I, II).
The most important property is determined by the value of λ. If $\lambda < 1$, it follows from equation (21) that

$$S(t) \propto t^{1/(1-\lambda)} \tag{26}$$

It seems natural to expect that $\lambda = 1$ becomes the critical point. Hedriks et al. (1983) has proved that mean mass evolves as

$\lambda < 1$ Power-low growth
$\lambda = 1$ Exponential growth
$\lambda > 1$ Gelation (Runaway growth)

Here, what does "Gelation" or "Runaway Growth" mean for third class? It should be noted the latter word is a jargon in the field of planetary sciences. In this paper, we will use both words case by case. An instructive example of "Gellation" is given by the product kernel as follows. Multiplying Eq. 9 by k and summing up from 1 to ∞, we can obtain the equations for time development of the moment

$$\frac{dM_n}{dt} = \sum_{i+j=k} K_{ij} n_i n_j (\{ (i+j)^n - i^n - j^n \} \tag{27}$$

one can easily derive following results for product kernel

$$\frac{dM_2}{dt} = M_2^2 \tag{28}$$

With a initial condition that $M_2(0) = 1$, the solution is given by

$$M_2 = \frac{1}{1-t} \tag{29}$$

Since the second moment represents the mean mass in the system, its divergence within finite time t_c (= 1 in this example) indicates the appearance of infinite-sized cluster in the system. This is the phenomenon called "gelation". Even with gelation, a different types of scaling relation holds for the size distribution near and after t_c. We refer to Ernst et al. (1985) and Hendriks et al. (1983) for further detail.

In order to investigate the evolution of the system after t_c, we must specify the sol-gel interaction (Ziff and Stell 1980, Ziff 1980). In other words, the mass flux from the sol to the gel phase must be modeled on the physical basis. Multiplication of coagulation equation with k and summation over all $k << L$ gives an equation for the mass flux from clusters of size $k < L$ to clusters larger than L:

$$J(L,t) = -\sum_{k=1}^{L} k\dot{N}_k = \sum_{i=1}^{L} \sum_{j=L-i+1}^{\infty} iK_{ij}N_iN_j \tag{30}$$

In the pre-gell stage ($t < t_c$), where the mean cluster size is finite and large clusters are relatively rare, the mass flux vanished as L$\rightarrow \infty$, i.e., $J(\infty, t) = 0$. Consequently, the mass conservation holds for only with the sol mass for $t < t_c$

$$M_{sol} = \sum_{k=1}^{\infty} kN_k = \text{constant} \tag{31}$$

At the gel point, or in generall for all $t > t_c$, $N_k(t)$ falls off algebraically, not exponentially, so that $J(L,t)$ approaches a finite, non-vanishing limit as $L \rightarrow \infty$. Therefore, there exists a non-vanishing mass flux $J(\dot{L},t) = -\dot{M}(t)$ from the sol to the gel phase and the mass conservation is replaced by

$$M_{sol} + M_G = \text{constant} \tag{32}$$

where M_G represents the mass of the gel. Thus, equation (27) after t_c should be replaced with

$$\frac{d}{dt}(\sum_{k=1}^{L} k^n N_k) = \frac{1}{2}\sum_{j=1}^{L}\sum_{i=1}^{L-j} K_{ij}N_iN_j(\{\ (i+j)^n\ -\ i^n\ -\ j^n\ \} - J_n(L,t) \tag{33}$$

where $J_n(L,t)$ is

$$J_n(L,t) = \sum_{i=1}^{L}\sum_{j=L-i+1}^{\infty} i^n K_{ij}N_iN_j \tag{34}$$

Namely, the critical point is marked by not only the moment divergence but also the onset of a mass flux from the finite-sized cluster (sol) towards the cluster of infinite size (gel). The problem how to model this mass transfer will be discussed later in section (5.4).

Subsequently, we divide the non-gelling coagulation equations ($\lambda < 1$) into subclasses by the value of μ. CLASS I,II and III corresponds to the case for $\mu < 0$, $\mu = 0$, $\mu > 0$, respectively. Levvraz (1986) indicated that Class I kernels give the power-law at the lower end of the size distribution while bell-shaped size distributions are realized with Class III kernels. The behavior of Class II kernels, which are quite important in realistic applications as we will see in the next chapter, are more complex and depends on the property of the kernel. But if $\mu = 0$, $\nu = \lambda = 1$ (van Dongen 1987 II), their behavior is similar to that for Class I, i.e., power-law size distribution. But the exponent τ cannot be directly related to the homogeneity exponents. The relation between these scaling functions and the exponents are listed in table (4). We refer van Dongen and Ernst (1988) for more detail. Figures 14 and 15 show the evolution of the size distribution with following two test kernels

$$K_{ij} = (ij)^{1/4} \quad \text{(Class I)} \tag{35}$$

$$= i^{-1/4}j^{3/4} + j^{-1/4}i^{3/4} \quad \text{(Class III)} \tag{36}$$

Each plot is drawn when the total cluster number becomes the half of the previous epoch: i.e., 1/2,1/4,1/8,1/16, times initial particle number. Unless the interval is specified explicitly, all following figures in this paper are drawn in the same manner. Although the lower tails of the distribution show different behavior, the mean size increase in a similar way because they share the common exponents λ (fig.16). In figure 17, the numerical calculations are compared with the prediction based on scaling assumptions. One can see the excellent agreement. Also, an experimental evidence of dynamic scaling is reported by Broide and Cohen (1990). However it should be noted that the results obtained with scaling property have the status of a conjecture to some extent and cannot rule out completely different asymptotic behavior.

The difference between Classes can be understood as follows. Since the value of exponent μ is positive for Class I kernels. larger aggregates preferentially accrete equally large ones, leaving a poly-disperse system (power-law) behind. Contrary with Class III kernels ($\mu < 0$), the system remains fairly monodisperse as large aggregates grow first by eliminating small aggregates. This rather intuitive explanation for the difference between Classes has a profound implication in answering the question raised at the end of chapter 2. Here, we restate the question :
"What kind of aggregates are resulted from a certain coagulation process?"

Figure 14:

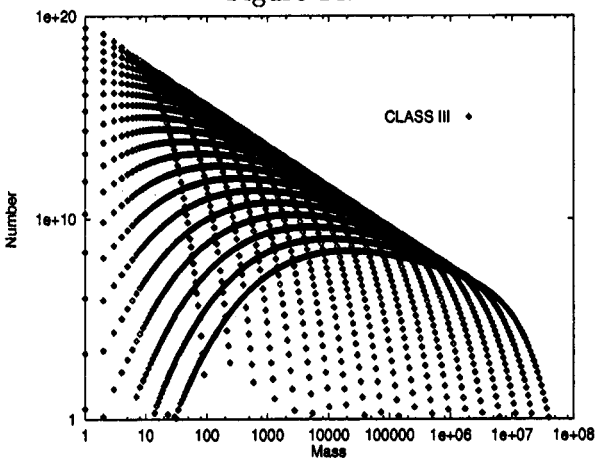

Evolution of the size distribution for Class III test kernel.

Figure 15:

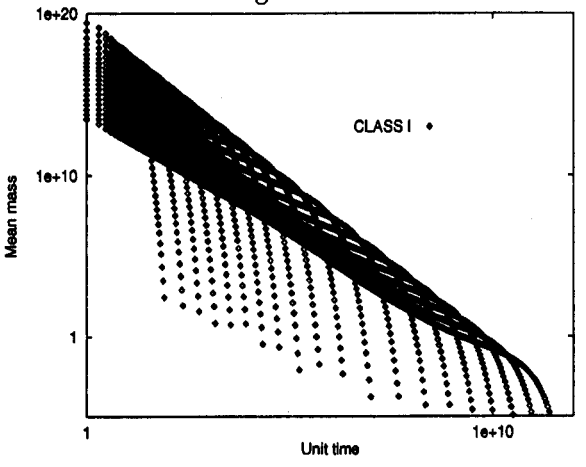

Same as Fig.(14) but for Class I test kernel

Figure 16:

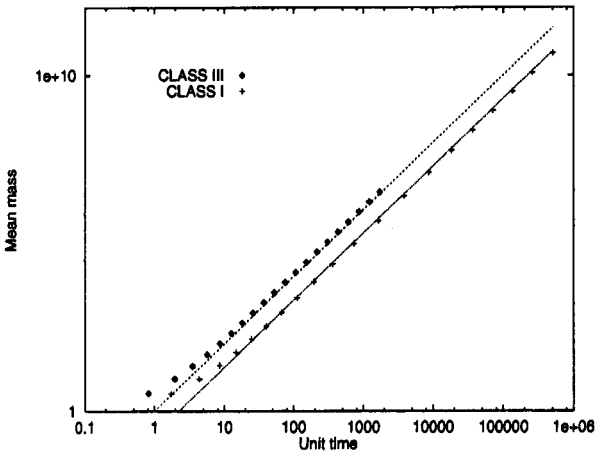

Time development of mean cluster size. Both fitted curves are proportional to t^2.

Figure 17:

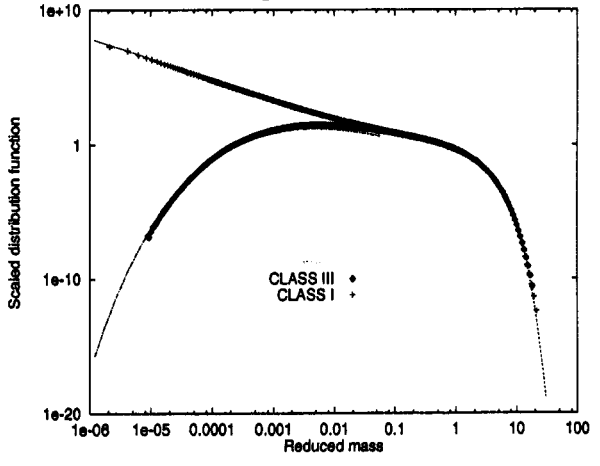

Scaling function for each kernel. Fitted curves are drawn using the scaling theory (see table 4).

Table 4:

CLASS	μ value	Small x behavior
I	>0	x^τ $(\tau = 1+\lambda)$
II	$=0$	x^τ $(\tau = 2 - p_\lambda/w)$
III	<0	$exp(-x^{-\lvert\mu\rvert})$

Properties of scaling functions. w is a separation constant and $p_\alpha = \int_0^\infty x^\alpha \Phi(x) dx$ (van Dongen and Ernst 1985 II) Large x behavior can be expressed with $\Phi(x) \sim x^\lambda exp(-zx)$ universally (van Dongen and Ernst 1987 I).

Intuitively, it is expected that the bell-shaped size distribution for Class III kernels yield cluster-cluster aggregates. Since we obtain $S(t) \sim K_{S,S}$ from eqs.17 and 21, one can see that collisions between two aggregates of typical size are dominant to change mean cluster size distribution. Naturally, this leads to the formation of fluffy aggregates like BCCA. On the other hand, it is somewhat uncertain what kind of aggregates are formed from Class I kernels. One may expect BPCA for power-law size distribution because only large aggregates at the upper tail of size distribution grow, consuming smaller aggregates. But this argument is not true because larger aggregates preferentially collide with equally large ones as noted earlier ($\mu > 0$). It means that large aggregates are formed by piling up smaller aggregates (of course not always equal-size) step by step even with Class I kernels. With Class III kernels, the whole system evolves with the peak of the bell-shaped size distribution, whereas most of the mass is concentrated in the upper-tail of the power-law distribution is for Class I kernels. Hence, the collisions between larger and smaller particles than the peak have negligible contribution to change the mean mass for CLASS III kernels. From these consideration, we may conclude that filamentary aggregates, such as BCCA, are generally produced in coagulation processes unless gelation (runaway growth) occurs. This preliminary conlusion will be checked further in section (4.4) by Monte Carlo simulations.

We classified the kernel using the values of μ and λ in this section. A classification with ν values will be considered in section 5.4 in conjunction with the system size dependence of the onset of gelation. Moreover, Scaling formulation has been extended to coagulation with injection (Hayakawa and Hayakawa 1988, Hayakawa 1987) and coagulation with fragmentation processes. (Meakin and Ernst 1988, Elminyawi et al. 1991) Finally, we remark that the results based on homogeneous kernels assumption (eq.17) is also valid for asymptotically homogeneous kernels, with the property $K_{ij} \sim \lim_{a\to\infty} a^{-\lambda} K_{ai,aj}$.

4.3 Numerical scheme

In this section, we present the detail of our code to solve coagulation equation numerically. If the mass distribution is linearly divided, the number of necessary bins becomes unacceptably large to cover the tremendous wide mass range of interest (FrenKlach and Harris 1987). Several techniques have been developed to reconcile the computational cost with the accuracy and numerical stability, such as sectional method (Bleck 1970) and J-space transformation method (Berry 1967).Extensive comparative studies can be found in Seigneur et al. (1986) and Tohno (1995). The common basic idea in these methods is the static division of mass coordinates in logarithmic scale. In contrast to these fixed mass-coordinate algorithms, Wetherill and Stewart(1989) has presented the numerical scheme with a number of "moving" batches, While usual methods use fixed mass bins to represent the actual size distribution, their "Lagrangian-type" approach employs the batches with variable width. A crucial attribute of this algorithm is the probabilistic procedure used to simulate abrupt changes

in the mass of the largest body. During a time step of length Δt, the collision number between i-mer and j-mer is given by

$$\nu_{ij} = N_i N_j k_{ij} \Delta t \tag{37}$$

Usually, this number becomes quite large and express the decrease of the number of i-mer and j-mer and the increase of the destination batch of (i+j)mer. However, the value of ν_{ij} often falls between 0 and 1 if i-mer and j-mer represent very large bodies. In this case, it is physically reasonable to interpret a fractional value of ν_{ij} as a collision probability per time step. Thus, the procedure creates a new batch containing one body only when $m_i + m_j$ exceeds the mass of he largest body by a preassigned factor δ. and ν_{ij} exceeds a random number between 0 and 1. Thus, this algorithm can be regarded as a hybrid of the probabilistic (Monte Carlo) and deterministic (coagulation equation) approach. At first glance, the formulation of the algorithm may seem to be rather heuristic, not mathematically rigorous. However, the algorithm can describe the evolution of mass distribution very accurately, even for gelling model as shown below. Consequently, we employ this algorithm with $\delta = 1.1$ to solve the coagulation equation throughout this paper.

As pointed out by Ohtsuki et al.(1990), it is quite important to check the accuracy of numerical calculation by the comparison with analytical exact solutions. They have shown that calculations with a fixed mass-ratio between neighboring mass coordinates more than $\sqrt{2}$, can substantially overestimate the number of bodies at the tail of mass distribution. Figures 18 $\sim$ 21 show the results of our simulation. The initial monomer number is 10^{20}. One can see excellent agreement between the results of numerical simulations and the corresponding exact analytic solutions. In particular, calculations for product kernel have special meaning to examine the capability of a numerical scheme because it provides only one analytical example of gelation (runaway growth).

4.4 Monte Carlo simulations

As we found in chapter 2, the kinetics of coagulation process plays an important role to determine the geometry of the resulting aggregates. On the other hand, the actual shape of the aggregate controls the kinetics through the collision rate depending on the gas drag force. It is likely that the actual aggregation process consists of a combination of two extreme cases, namely BPCA and BCCA. We must examine the both aspects in a self-consistent scheme in which a pair of clusters is merged with ballistic trajectories according to the collision probability. Recently, two-dimensional coagulation equation has been developed to investigate the geometry and the kinetics simultaneously. It can treat not only the mass, but another parameter, such as porosity (Ossenkopf 1993) or surface area (Xion et al. 1993), as the physical quantity to specify the shape of the aggregates. However, we concern the traditional approach, i.e, Monte Carlo method in this section (Sutherland 1967, Sutherland and Goodarz-Nia 1971).

In general, Monte Carlo method (MC) is regarded as an approximation to follow the coagulation equation. But this view is a complete misunderstanding since MC is based on more fundamental representation of actual physical processes including intrinsic fluctuations, i.e., Master equation. Actually, Gillespie (1975) proved that MC with an appropriate algorithm can faithfully follow the time-development of the system described by Master equation. It is well-known that Gillespie's algorithm gives most rigorous procedure among several variations of algorithms for MC calculations (Lapidus and Shafrir 1972, Ryan et al. 1975). The algorithm has been originally developed to describe warm rain formation (1975), later applied to follow stochastic nature of coupled chemical reactions (1977).

Figure 18:

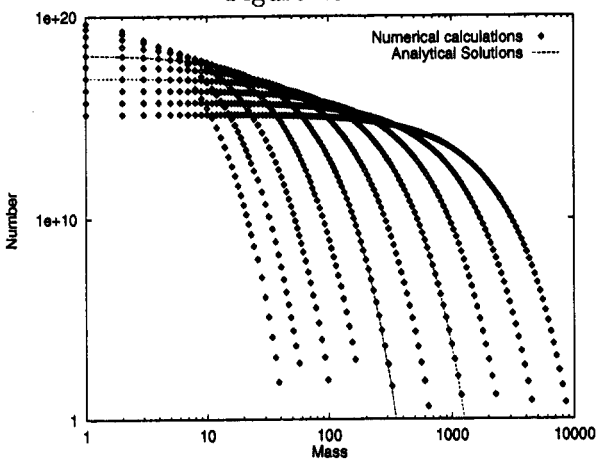

A comparison between numerical calculations and analytical solutions for constant kernel $K_{ij} = 1$. Each line for numerical calculation denotes 1,2,4,....64 in unit time.

Figure 19:

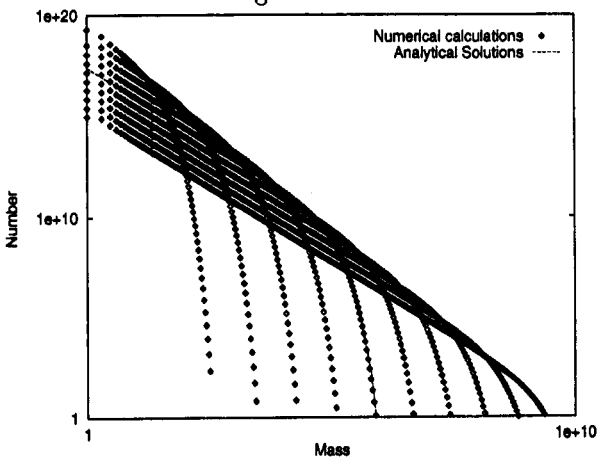

Same as Fig.(18) but for sum kernel $K_{ij} = i + j$. The interval between two adjacent lines is 1 in unit time.

Figure 20:

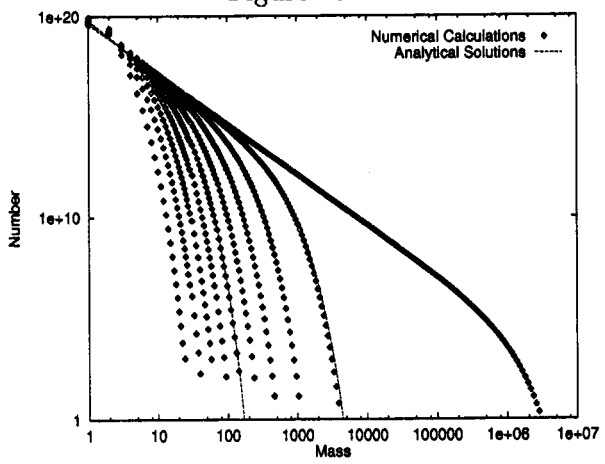

Same as Fig.(18), but for product kernel $K_{ij} = ij$ before the onset of runaway growth. The interval between two adjacent lines is 0.1 in unit time.

Figure 21:

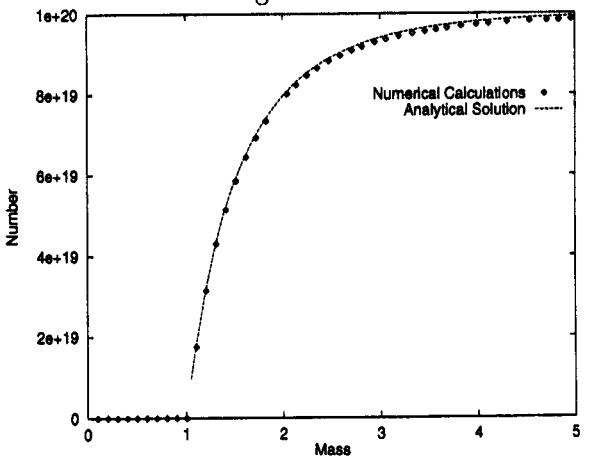

Time development of largest mass for the product kernel.

See the review by himself for the detail of this scheme (1992). Since the implementation of this scheme has not been completed yet unfortunately, we currently employed a much simpler algorithm for MC by Meakin (1991). Using the MC simulations, we study the effect of collision kernel on the geometry first. Subsequently, we extend our simulations to account for interactive evolution of the geometry and kinetics.

Probably, the paper by Botet et al. (1984) was the first attempt to investigate the effect of the dynamics on the shape of the aggregates using Monte Caro method. They consider the coagulation described by the following kernel

$$K_{ij} \propto (ij)^{\omega} \tag{38}$$

Clearly, BPCA (BCCA) correspond to the case where $\omega \to \infty$ ($\omega \to -\infty$), since only a largest cluster (smallest clusters) in the system can move. Changing the exponent ω, they observed sudden transition from CCA to PCA at $\omega = 1/2$. As we see in section 4.2, this point ($\lambda = 2\omega = 1$) corresponds to the boundary between orderly growth and runaway growth. Their results suggest that the fractal dimension of the aggregate remains almost same as BCCA ($D \sim 2$) if the growth proceeds orderly. But once gelation (runaway) occurs, the dimension shall increase to 3 (BPCA). Subsequently, Meakin and Donn (1988) reported the results of similar simulations with various exponent determining mass dependence of the velocity,i.e. $v \sim mass^{\omega}$. The values of ω -1, -1/2, 0 and 1/2 yielded the fractal dimension 1.95, 1.95, 2, 2.2, respectively. These previous works seem to support our preliminary conclusion presented in section 4.2 that fractal dimensions of the aggregates becomes about 2 insensitive to the detail of coagulation processes. But these previous works include several problems to be validated.

Main difficulty in the study by Botet et al. lies in the rather small number of total particles in simulations. They obtained only one big cluster containing all particles in the system at the end of the simulations. Although they repeated the simulations with same initial condition to reduce the statistical uncertainty, the kinetic aspect of the coagulation process become meaningless at the later stage with small total cluster number. This problem is irrelevant to Meakin's work since the total number of particles in the system is taken substantially large at expensive computational cost. However, he gave no verification whether his code describe the kinetics correctly. As we employ Meakin's algorithm for our simulations, the brief description is made to explain why it gives correct time development.

In this scheme, simulations start from a list of N single-particle. A pair of clusters (i-mer and j-mer) is selected at random. When a random number x ($0 < x < 1$) is larger than K_{ij}/K_{max}, where K_{max} is the largest value of K_{ij} for any pairs of clusters in the system, two clusters are returned to the list. When $x < K_{ij}/K_{max}$, the two clusters are combined with the same procedure as BCCA. If two clusters miss each other (only for fluffy aggregates), they are returned to the list. It follows that abundant clusters with larger collision probability is preferentially selected in this procedure. How can we introduce the time dependence? Substituting n = 0 in eq.27, we get

$$\frac{dN_{total}}{dt} = -\frac{1}{2}\sum_{i}^{\infty}\sum_{j}^{\infty} K_{ij} n_i n_j \tag{39}$$

Setting $dN_{total} = 1$, the time for a next collision is expected to be

$$2/\sum_{i}^{\infty}\sum_{j}^{\infty} K_{ij} n_i n_j \tag{40}$$

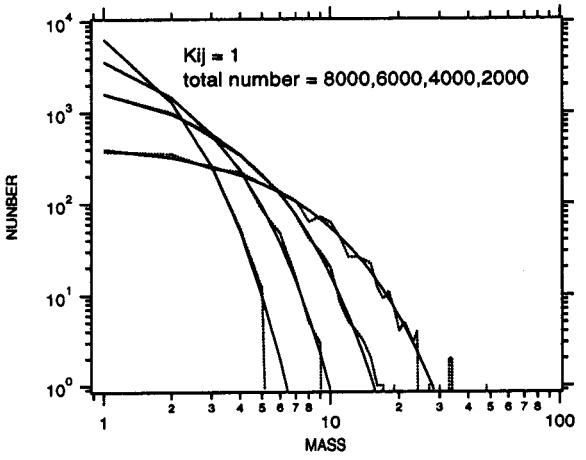

Figure 22:
Comparison between the Monte Caro simulations and the corresponding analytic solutions. The case for constant kernel .

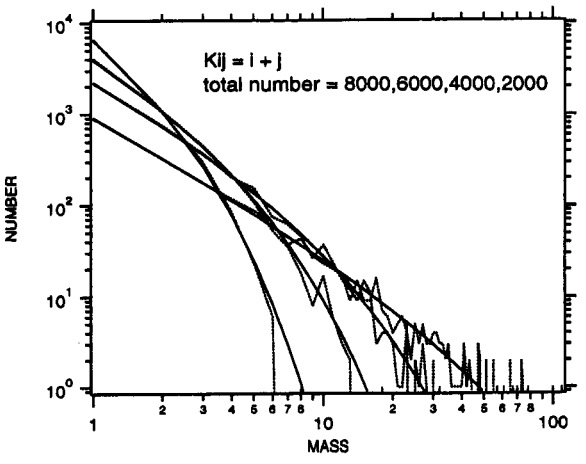

Figure 23:
Same as fig. 22, but for sum kernel.

On the other hand , the probability for for creating one new cluster with one trial is given by

$$\sum_{i}^{\infty}\sum_{j}^{\infty}\frac{K_{ij}}{K_{max}}\frac{n_i}{N_{total}}\frac{n_j}{N_{total}} \tag{41}$$

with the procedure described above. The inverse of this quantity is the expected number of trial to produce one cluster, in other words to decrease total cluster number by 1. Therefore, our procedure coincides with eq.39 completely if the time increment for each trial is set equal to $\Delta t = 2/(K_{max}N^2{}_{total})$. irrespective of whether or not they are actually combined. Again, we tested the code by the comparison with exact solutions. Although it is preferable to use exact solutions of Master equation, we content ourselves here with the solutions of coagulation equation. (figs.22 and 23). From these figures, we can confirm that our code with Meakin's scheme can describe the kinetics of coagulation accurately. However, practical computational problems, such as long CPU time and huge memory requirement, arise if we consider large number of particles in the system. Recently, Liffman (1993) proposed a new MC scheme which can trace the evolution of cluster size distribution correctly. Since the "Topping up" technique used in his calculations is quite effective to reduce the computational cost, we incorporate this into Meakin's scheme.

First, a subsystem containing $10^4 \sim 10^5$ randomly distributed test particles is considered (see Fig.24). If coagulation is continued for a long time, the number of clusters in the subsystem will decrease to a point where the results will become statistically unreliable. In order to prevent this statistical fatigue, we simply double the number of clusters in the subsystem, which is equivalent to adding an exact copy of the subsystem to itself. This procedure is based on an assumption that the behavior of the subsystem is an indicator of that for whole system This assumption must be tested since the fluctuation in the subsystem may be amplified by this procedure. In figure (28), the size distributions for thermal coagulation , with and without topping technique, are compared. In addition, we checked the results of calculations with topping technique by the comparison with analytic solutions (figs. 25 and 26). Note the wide mass range in comparison with the calculations without

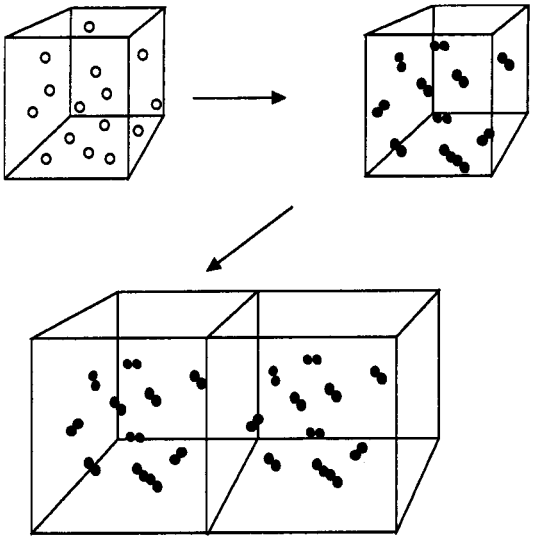

Figure 24: Schematic for "Topping" technique. The MC code can only examine a reasonably sized system containing $10^4 \sim 10^5$ particles at a time. Thus, we consider a subsystem (upper left box) of the total system and assume that the behavior of the subsystem duplicates the system as a whole. It is important that a robust number of clusters be resident in the subsystem , since the errors in the simulations goes like the square root of the total cluster number. As clustering proceeds, the total number of clusters within the subsystem must decrease (upper right box). When the number of clusters becomes too small, the system is "topped up": i.e., we add the subsystem to the duplication of itself (lower boxes).

topping (figs. 22 and 23).

In summary, our code based on Meakin's scheme with "topping" technique can accurately follow the evolution of the system containing vast number of particles (up to $\sim 10^7$). Using this code and test kernels with $K_{ij} = (i+j)^{\omega}$, we have examined the effect of the kinetics on the shape of the aggregates. These are rather simple cases because the collision kernels are determined in advance. In other words, preassigned collision kernels are not affected by the geometry of resulting aggregates. Figure 30 shows the relation between the maximum radius and mass for sum kernel ($\omega = 1$). Every symbol denotes the number of constituent particles and the maximum radius for individual aggregate. The fractal dimension is computed by the curve fitting on this figure. We obtained similar values for different exponents ω (fig. 27).

Next , we investigate more realistic and complicated situations where the kernels are influenced by the geometry of aggregates. In this interactive model, the collision rate is computed from the actual cross section and the relative velocity. Because of the variation in the shape, the cross section term in the collision rate is not uniquely determined even for the aggregates of same mass. Memorizing maximum radius of every aggregates, however, we can easily calculate the cross section term. On the other hand, it is generally difficult to calculate the relative velocity term because we need to estimate more complicated properties of the aggregates, e.g., the ratio of mass to projected area for settling or turbulence induced relative motion. At present, the cross section estimate for all aggregates is too time-consuming to incorporate into the simulation. Therefore, we consider only one simple case in this section, i.e., the coagulation driven by the thermal motion of the aggregates. In this case. the relative velocity term between i-mer and j-mer is $\sim \sqrt{1/i + 1/j}$ irrespective of the geometry of the aggregates. Figure 31 shows the relation between the maximum radius and the number of constituent particles in the aggregates. When the system is "topped up", we plot the every aggregates on this figure. Different symbols represent the different stages of the coagulation. A least square fitting yields the relation

$$Rmax = 0.765 N^{0.543} \tag{42}$$

Again, we found fractal aggregates with D $\sim$ 2. Several examples of the aggregates generated in

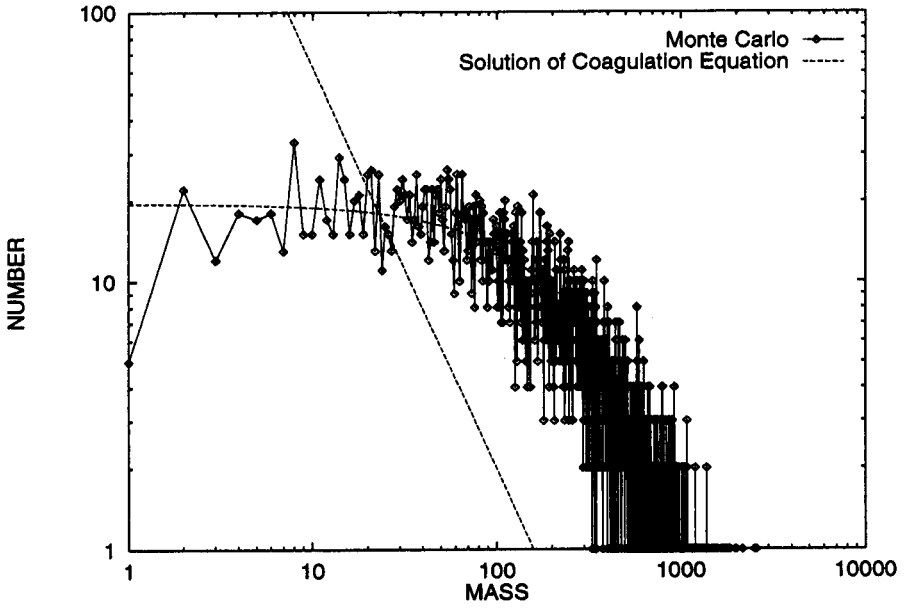

Figure 25:
Comparison between the Monte Caro simulations with topping and the corresponding analytic solution of coagulation equation. The case for constant kernel

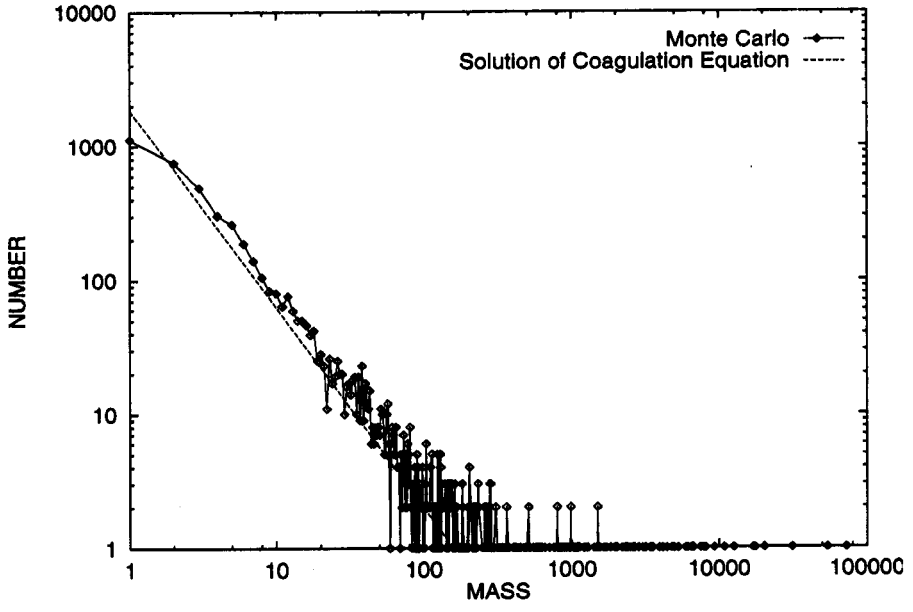

Figure 26:
Same as fig. 25, but for sum kernel

Figure 27:

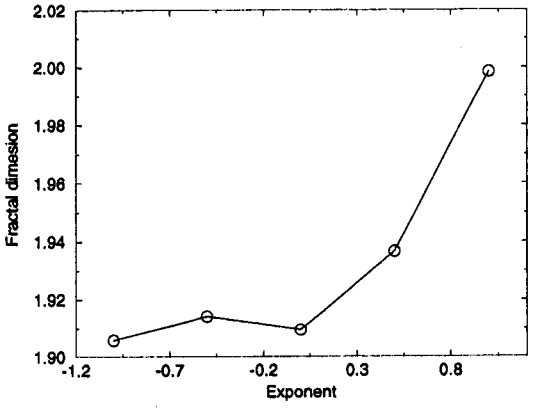

Fractal dimension versus the exponent ω.

Figure 28:

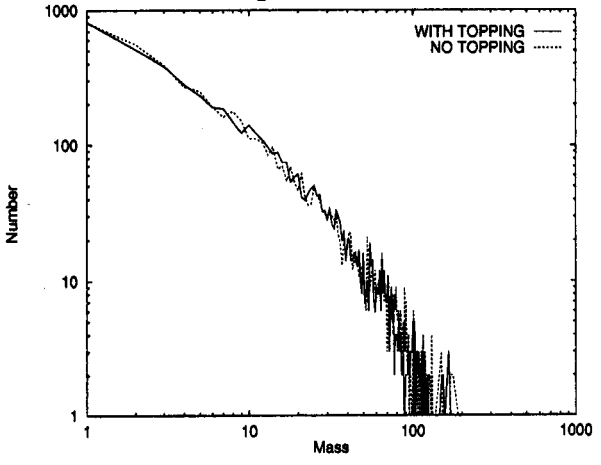

Size distribuions for thermal coagulation with and without topping.

thermal coagulation are displayed in Fig.32. Apparently, they are quite similar to BCCA.

In conclusion, we have confirmed our prediction in section 4.2 with Monte Carlo simulations. That is, all orderly growth (even with power-law size distribution) lead to the formation of fluffy aggregates uniformly having fractal dimension ~ 2. If this observation holds for generally, it is no longer necessary to follow the structure of each cluster with MC. The coagulation equation, modified to account for the fractal geometry, provides more rapid and wide-ranged computations. In order to check the consistency between two methods, we compare the results of MC and modified coagulation equation in fig.(29). The discrepancy at lower size(k = 1,2,3 $\cdots$) can be attributed to the deviation of eq.(42) from the actual maximum radii for small aggregates. While the relation (42) is valid only for large aggregates in fractal limit, R_{max} for monomer should be 0.5 and 1 for dimer, trivially. In chapter 2, the effect of the kinetics on the geometry is studied using extreme simple models, namely BPCA and BCCA. On the other hand in the following chapter, we investigate how the geometry, characterized by a fixed fractal dimension, change the kinetics. However, these simplified strategy will fail if there exists complicated feedback between two aspects as suggested by Ball et al (1987). We plan to study the problem with rigorous Gillespie's code in near future.

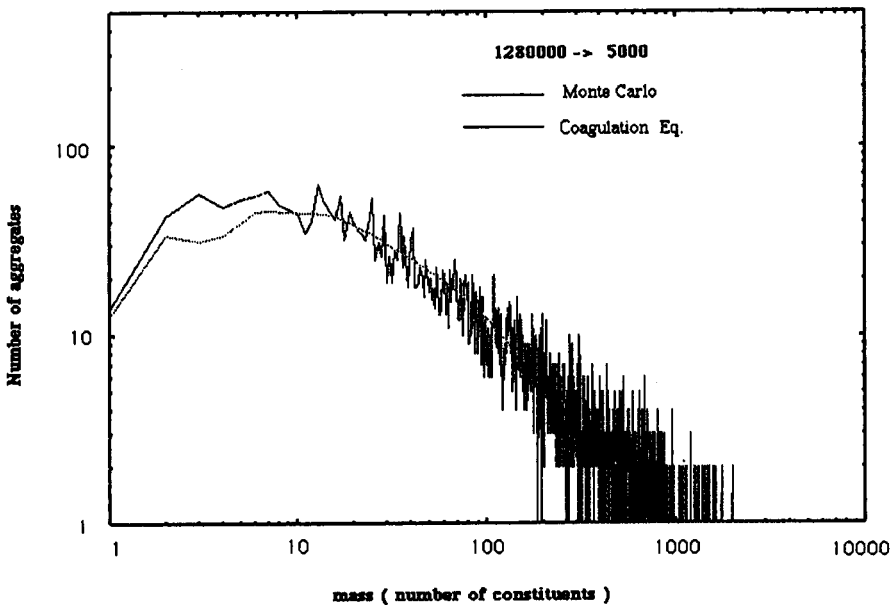

Figure 29: Comparison between Monte Carlo and Coagulation equation for thermal coagulation

5 Coagulation of fractal aggregates in the protoplanetary disk

There are various sources which yield a relative velocity between the dust particles in a protoplanetary disk. For very small grains , the thermal motion of grains dominates their relative velocities. As the size grows, other effects, such as settling, radial drift and turbulent motion become important through the gas interaction (fig.33). The relative importance varies locally and temporally dependent on the position in the disk and on the size of the particle (see figs.34 and 35). As we found in the previous chapter, fractal dimension of the aggregates can be approximated by 2 for any kinds of coagulation processes useless a runaway body forms. Once we determine the fractal dimension of the aggregates, collision kernel can be modified in a simple manner to account for the geometry. The cross section term is calculated by simply replacing $(i^{1/3}+j^{1/3})^2$ with $(i^{1/D}+j^{1/D})^2$. In this section, we set the fractal dimension as 2. Moreover, we can calculate the velocity term based on the "area-equivalent sphere approximation" validated in section 3.4 if we know the cross section of fractal aggregates. Several authors (Ossenkopf 1993, Meakin and Donn 1988 Mukai et al. 1992) have formulated the relation between the ratio of the mass to the projected-area m/A. Among them, we employed Ossenkopf's formula to calculate the values of m/A for fractal aggregates. This is derived from the fitting for BCCA which we regard as representative of fractal aggregates with D $\sim$ 2. When the number of constituent particles N is less than 30

$$m/A = 1/(15.2N^{-1/3}\exp(-2.86/N^{0.096})) \tag{43}$$

and for N $\geq$ 30

$$m/A = 1/(0.692N^{-0.05}\ (1+0.301/\log N)) \tag{44}$$

Though this formula gives much less mass dependence of the cross section compared with sphere ($N^{1/3}$), the exponent is not zero, but 0.05 in the limit N $\rightarrow \infty$. Theoretically, this weak dependence

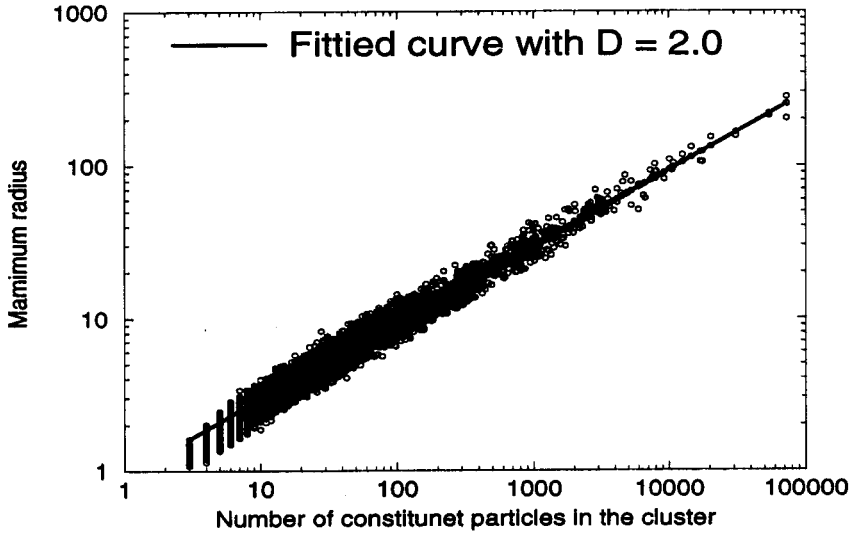

Figure 30:
Rmax versus N for sum kernel

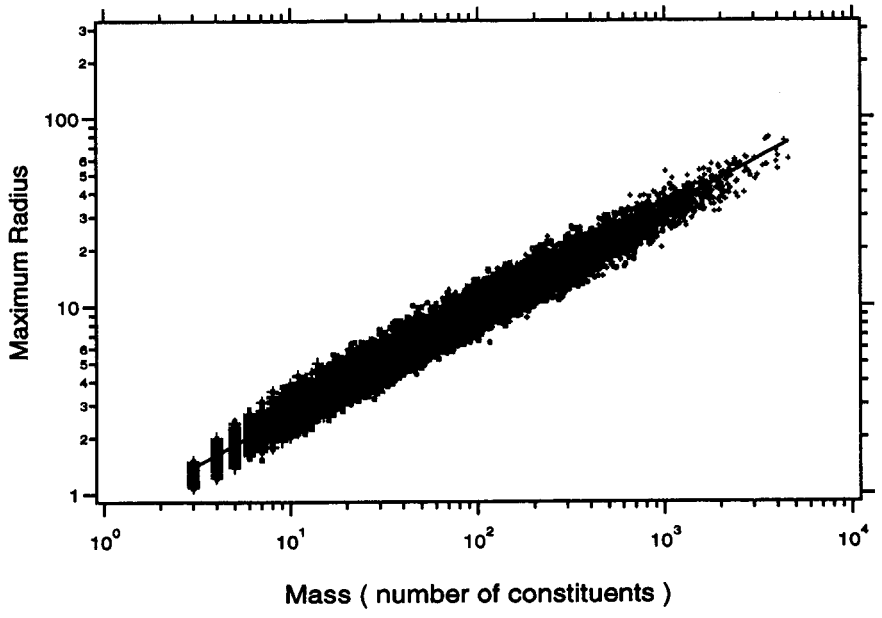

Figure 31:
Same as fig.(30), but for thermal coagulation

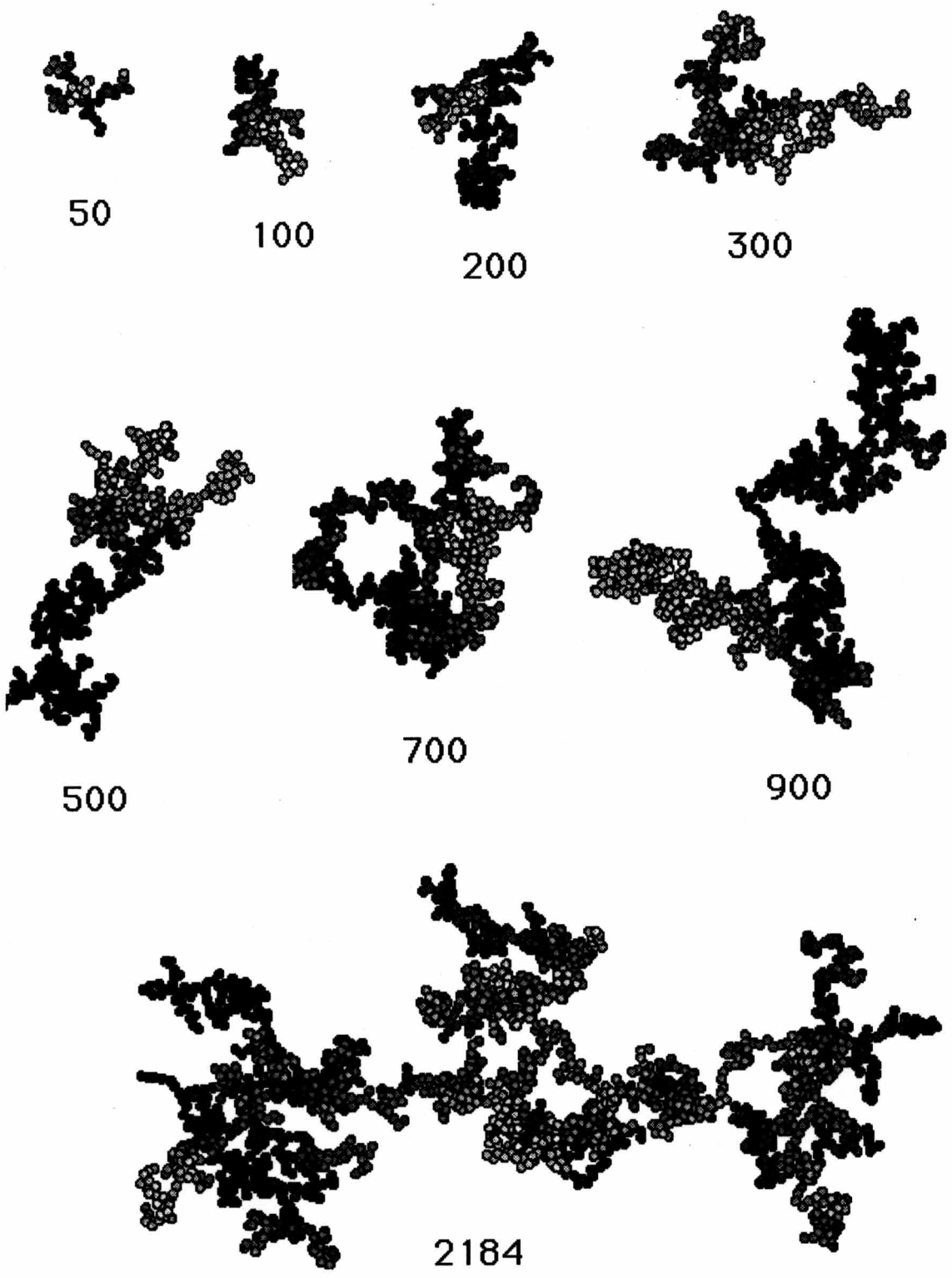

Figure 32:

Examples of the aggregates produced by Monte Carlo simulations for thermal coagulation

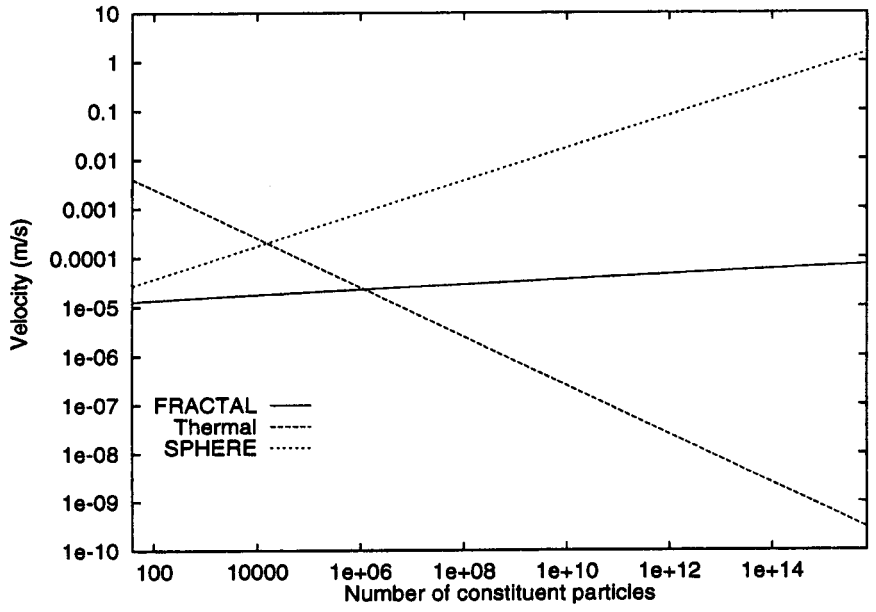

Figure 33:

Thermal and settling velocity for spheres and fractal aggregates. The radius of the consituent is 0.1 μm and the disk paramters are adopted from table 5

may be criticized because the ratio should approach 1 for the aggregates characterized by the fractal dimension less than 2, such as BCCA (Meakin 1991). It should be noted even the largest clusters used for fitting in Ossenkopf's calculation include at most about 16000 constituent particles. Plugging this formula and modified cross section in the kernel, we will investigate the effect of the fractal geometry on the kinetics in the following sections.

5.1 Thermal coagulation

The "reaction time" t_f defined in chapter 2 can be interpreted in a different way,, i.e., "thermalization time" for the dust particle. Comparing this time scale with that for dust-dust collision, Hayashi and Nakagawa (1975) found that the velocity distribution of grains becomes almost Maxwellian distribution due to the collisions by gas molecules under the condition of a typical protoplanetary disk. Thus, the collision kernel for thermal coagulation is

$$K_{i,j} = (i^{1/D} + j^{1/D})^2 \sqrt{(\frac{8kT}{\pi m_0})(\frac{1}{i} + \frac{1}{j})} \tag{45}$$

Figures 36 and 37 show the evolution of the size distribution for spherical and fractal growth, respectively. According to the arguments in section 4.2, we find $\mu = -1/2 < 1$, $\nu = 2/D$ and $\lambda = 2/D - 1/2 < 1$ (D = fractal dimension) for these cases. Actually, bell-shaped size distributions are realized for both cases as we expected. Lai et al. (1972) investigated the coagulation of spherical aerosol particle in the free-molecule limit. They proposed the concept of self-preserving spectrum originally introduced for the coagulation in continuum regime. This is a variation of the scaling function $\Phi(x)$ in which the mean cluster size is defined as $S = M_1/M_0$. Since the mass range in their numerical

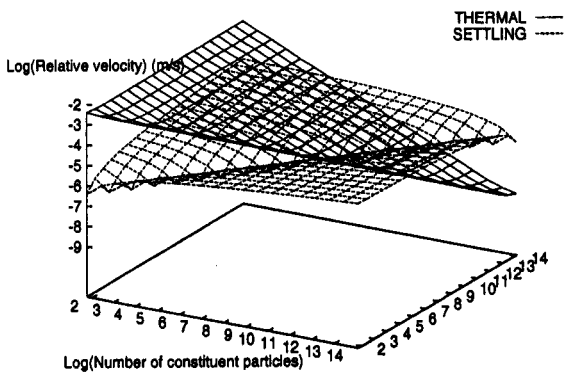

Figure 34:
Settling-induced relative velocities for fractal aggregates

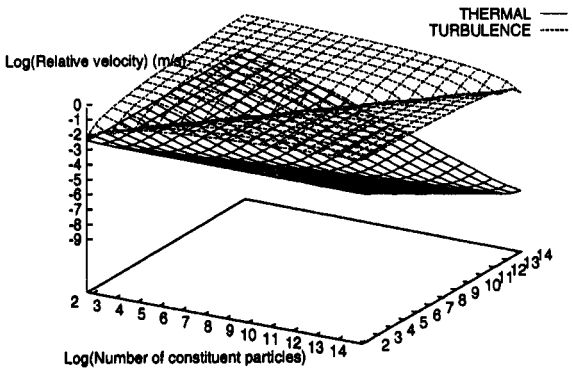

Figure 35:
Turbulence-induced relative velocities for fractal aggregates

calculations was not wide enough, they derived the self-preserving spectrum by the comparison of eq.(20) with their numerical calculations. Vemury et al. (1994) recently calculated the same problem with Discrete-Sectional method. In this method, the smaller particles are treated as discrete entities, while the large ones are grouped in sections. Thus, the self-preserving spectrum can be obtained accurately with direct numerical calculations. Their results are compared with our calculation in fig.39.

What effects are caused by the variation of the dust geometry? First, fractal growth proceeds more rapidly than compact growth due to the enhancement of the cross section (fig.38). The asymptotic behaviors can be fitted by scaling assumptions, i.e., $\lambda = 2/D - 1/2$ and $S(t) \propto t^{1/(1-\lambda)}$. Also, we observed a wider self-preserving spectrum for fractal growth. This results qualitatively agrees with the previous studies (Wu and Friedlander 1993, Mulholland et al. 1988). For example, Williams(1990) investigated the effect of fractal particle structure on aerosol coagulation using moment analysis. He also found the trend of broader size distribution as fractal dimension decreases. Matsoukas and Frielander(1991) experimentally studied the dynamics of the metal oxide aggregates in the free-molecule regime. They also found the self-preserving size distributions for the metal oxide aggregates becomes wider than for compact spheres.

5.2 Turbulent coagulation

Most of previous research on turbulent disk have employed so-called alpha model in which turbulent viscosity ν_{turb} is parametrized as

$$\nu_{turb} = \frac{1}{3}\alpha H c \tag{46}$$

where H is the thickness of the disk, c is the sound velocity and α is a parameter less than unity representing the strength of the turbulence (Mizuno 1989). The equation (46) assumed that the size of largest eddies and r.m.s. velocity fluctuation are considered to be H and αc, respectively. There is a diversity of opinion as to the appropriate value of α. It ranges from 10^{-4} to 1 depending on the

Figure 36:

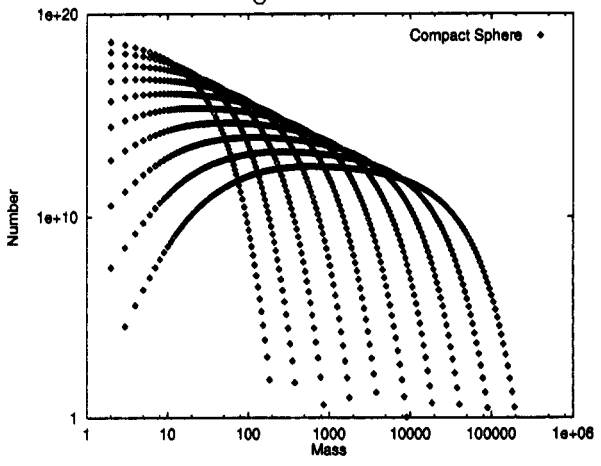

Time development of the size distribution for compact growth

Figure 37:

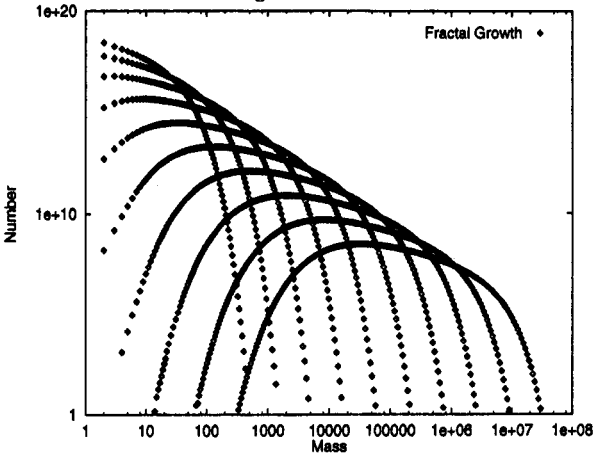

Same as fig.36, but for fractal growth

Figure 38:

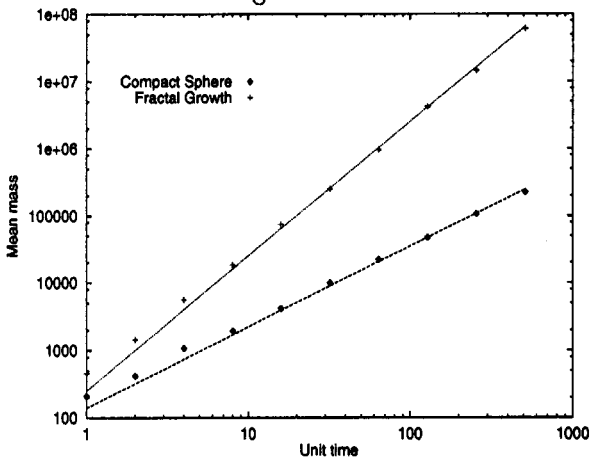

Mean mass evolution for the same epochs as in figs 36 and 37. Each fitted curve corresponds to $S(t) \propto t^{1.2}$ and $S(t) \propto t^2$, respectively.

Figure 39:

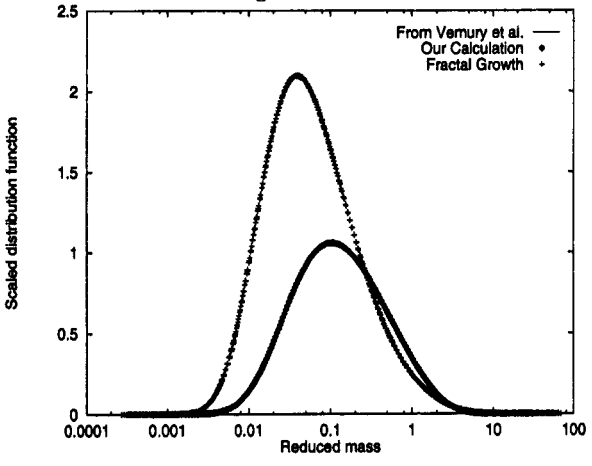

Our calculation by Wetherill's scheme shows complete agreement with the spectrum computed by Vemley et al. We can hardly distinguish them

Figure 40:

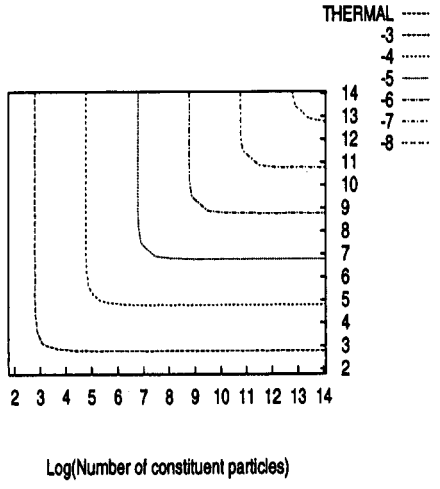

Contours of equal relative velocity driven by thermal motion of the particles. The size of a constituent particles is 0.1 μm and the number for each line denotes the logarithmic velocity in meter/sec. Since thermal motion depends on only the mass, a pair of particles have equal relative velocity irrespective of the geometry.

Figure 41:

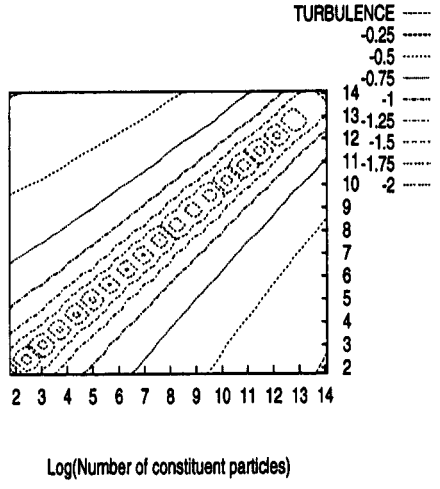

Turbulence-induced relative velocity for fractal aggregates based on the equation 52. Note the absence of the relative velocity between the aggregates of equal mass. This is because aggregates react with all eddies when $t_f < t_{in}$.

Physical quantities	Values	Unit in MKS
Hydrogen mass	1.66×10^{-27}	kg
Bolzman Constant	1.38×10^{-23}	J/T
Molecular Cross section σ	2×10^{-19}	m^2
1 AU	1.5×10^{11}	(m)
Half Thickness,H	0.042 AU	
Temperature,T	225	K
Gas density,ρ_g	5.7×10^{-6}	kg/m^3
Mean molecular weight μ	2.4× Hydrogen mass	kg/mol
Mass fraction of dust particles	0.0034	
Sound speed c ($= \sqrt{8kt/\pi\mu}$)	1410	m/s
Mean free path f ($=\mu/(\sigma\rho_g)$	0.0035	m
Viscosity $\eta(= cf\rho_g/3)$	9.36×10^{-6}	Pa*s
Reynolds number ($= \alpha cH\rho_g/\eta$)	5.41×10^{10}	

Table 5: Disk parameters adopted

mechanisms to drive turbulence (Mizuno 1989).

The energy in the largest eddies cascades through a spectrum of smaller eddies, down to a size where they are damped by molecular viscosity. Dimensional arguments imply that the energy dissipation rate per unit mass ε is

$$\varepsilon \approx u_{out}^3/l_{out} \tag{47}$$

On the other hand, the "inner" scales of the smallest eddies are given by

$$u_{in} \approx (\varepsilon\nu)^{1/4} = u_{out}Re^{-1/4} \tag{48}$$

$$l_{in} \approx (\nu^3/\varepsilon)^{1/4} = l_{out}Re^{-3/4} \tag{49}$$

$$t_{in} \approx (\nu/\varepsilon)^{1/2} = t_{out}Re^{1/2} \tag{50}$$

where Re denotes Reynolds number $\alpha cH/\nu$. On smaller scale, the flow is locally laminar, though varying with time. Assuming the Kolmogorov law for the turbulent energy spectrum for eddies with length scale between l_{out} and l_{in}, Völk et al. (1980) calculated the turbulence-induced relative velocity between the aggregates. The key parameters controlling the interaction between the dust aggregates and turbulence are the reaction time t_f, the inner time scale of the turbulence t_{in} and the turnover time scale of the largest eddies t_{out}. Putting the disk parameters listed in table 5 into eqs.(50) in (47), we obtain these two characteristic time scale of turbulence.i.e., $\tau_{in} \sim 2000$ sec and $\tau_{out} \sim 16$ year. Also, we remark that t_f is proportional to the radius when we consider spherical particles with uniform material density.

Draine gave an approximation formula for the relative velocity applicable to the case where the reaction time scale is larger than inner and smaller than outer scale of turbulence. The relative velocity, depending on the reaction time of larger particle only, is given by

$$u_{out}(t_f/\tau_{out})^{1/2} \tag{51}$$

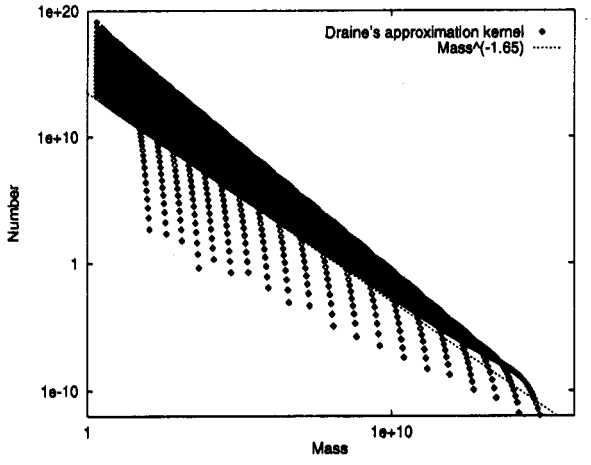

Figure 42:
Evolution of size distribution for the kernel with Draine's approximation. The fitted line has an exponent -1.65.

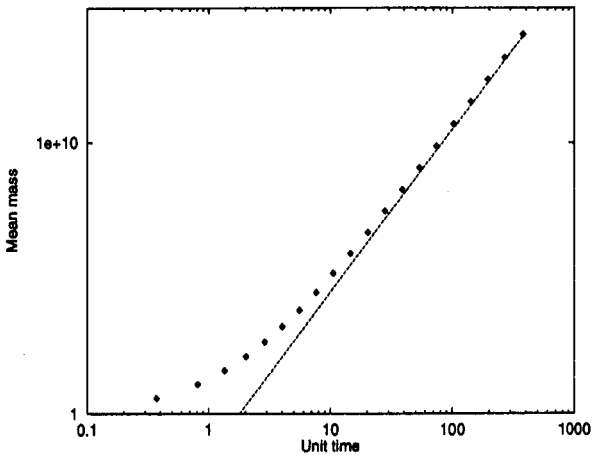

Figure 43:
Mean mass evolution for the same epochs as in fig.42 The dotted line represent the asymptotic behavior derived from scaling theory.

In spite of the simplicity, it agrees with more elaborated calculations by Völk et al. (1980). When t_f exceeds τ_{out}, the particles begins to decouple from the turbulent gas motion and the relative velocity for equal sized particles becomes $u_{out}(t_f \tau_{out})^{-1/2}$. For two aggregates with very unequal size, i.e., reaction time much larger than, and much smaller than τ_{out}, their relative velocity is almost constant and nearly equal to mean square turbulent velocity. We refer to Mizuno et al. (1988) for more detailed explanation. In this section, however, we consider only the case of $\tau_f < \tau_{out}$. Using Draine's formula, we have calculated the the evolution of the size distribution of spherical particles embedded in turbulent disk. The scaling theory predicts that mean mass grows as t^6 since the kernel has homogeneity exponents $\lambda = \nu = 5/6, \mu = 0$. Excellent agreement is seen in fig.43 after 10 unit time. The self-preserving spectrum seems to have the exponent -1.65 (figs. 42). Since the kernel belongs to CLASS II, it is rather difficult to find the relation between the value and homogeneity exponents immediately (see, table 4). Mizuno reported the value of 1.31 for upper part of the distribution. The discrepancy may be attributed to the difference of initial condition or the kernel approximation involved with Draine's formula.

Now, we turn to the case for $\tau_f < \tau_{in}$ where a particle is effectively coupled to all motions of the gas, down to the smallest eddies. If we consider the realistic fluffy aggregates, this regime is of direct relevance. Since the reaction time scale, proportional to the value of A/m, remains nearly same as that for a constituent particles for fractal aggregates, every aggregates in the system stay in the regime as long as t_f for a constituent particle is smaller than t_{in} and fractal growth continues. A careful analysis by Mizuno et al. (1988) has shown

$$v \approx \frac{u_i}{t_i} |\tau_{f1} - \tau_{f2}| \sqrt{\frac{\ln (Re)}{2Re^{1/2}} \frac{t_o}{\tau_{f1} + \tau_{f2}}} \tag{52}$$

Note that the velocity becomes relatively weak compared with the case for $\tau_f > \tau_{in}$ and the relative velocity vanishes for equal sized particles. When we consider the fractal growth, the enhancement of

the cross section is larger than offset by smaller relative velocity. Consequently, the growth mode is transfered to exponential and the mean mass evolution is considerably accelerated

5.3 Sedimentation and coagulation

Equation of motion for a particle with mass m and cross section A in a laminar disk can be written as

$$m\frac{dZ}{dt} = -(\frac{4\rho_g c\delta}{3A}) - (\frac{GM_\odot}{R^3})mZ \tag{53}$$

Here, δ denotes the correction factor for Epstein law dependent on molecule reflection mode. Besides, it includes the deviation from area-equivalent sphere approximation determined by the structure of the aggregates as discussed in section3.4. The location of the particle in the disk is determined by the heliocentric distance R and altitude Z from the midplane. Finally, the particles reaches its terminal velocity

$$V_Z = \omega^2 Z t_f \tag{54}$$

Since t_f is generally proportional to A/m , collision kernel for settling induced coagulation is

$$K_{i,j} \propto (i^{1/D} + j^{1/D})^2 \frac{1}{\rho_g c}|\frac{m_i}{A_i} - \frac{m_j}{A_j}| \tag{55}$$

First, let us examine the spherical growth. Figure 48 shows the time development of the size distribution for settling-induced coagulation. Apparently, it is quite similar to that for sum kernel indicated in figure 19. The similarity can be explained by the fact that both kernels belong to the same scaling class with $\lambda = \nu = 1, \mu = 0$. We can predict the effect of fractal geometry in the same way as we did in section 5.1 for thermal coagulation. Equation (55) can be approximated as

$$K_{ij} \propto A_j \frac{1}{\rho_g c}|\frac{m_j}{A_j}| \propto m_j \quad (i << j) \tag{56}$$

Namely, the values of the exponents ($\lambda = \nu = 1, \mu = 0$) remains same irrespective of the dimension of the particle.

Secondly, we consider the coagulation with the realistic kernels accounting for both thermal and settling motion of the aggregates (see figs 33 and 34). For spherical growth, the radius of a constituent particle is taken as 1 μm for the comparison with the calculation by Nakagawa et al. (1981). On the other hand, we set the size as 0.1 μm in the case of fractal growth . The unit time is 8.62 and 0.027 year, respectively. The difference must be borne in mind when we transform the unit time in the simulations to the real time scales. Initially, fractal growth proceeds much faster (t^2) than spherical growth ($t^{1.2}$) due to the larger cross section (fig.53). Both cases gradually move to the exponential growth stage where the relative velocity is dominated by settling ($\lambda = 1$). But the growth speed for fractal aggregates is smaller than that for spherical growth approximately by a factor of 6 (fig.52).

5.4 System size dependece of pattern formation onset

Dust settling to the midplane is a important process because the dust particles must concentrate in a thin layer to cause gravitational instability. A classical scenario by Safronov (1969) pays attention to the behavior of an exceptionally large particle in a system. As the particle falls through a field of smaller particles, it grows by sweeping them up. It follows from eq. (53) that the positive feedback

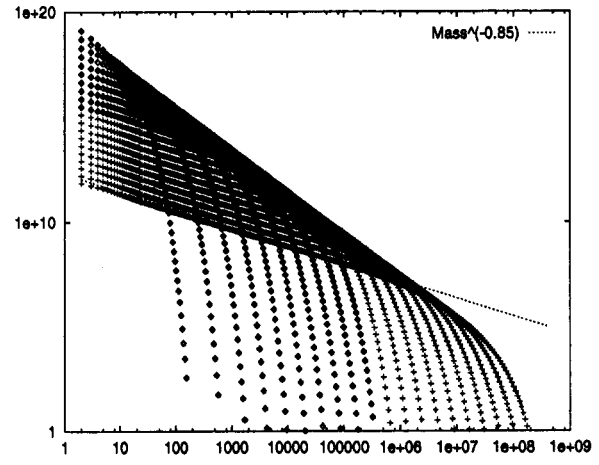

Figure 44:
Evolution of size distribution with the kernel represented by eq.(52) and spherical growth model

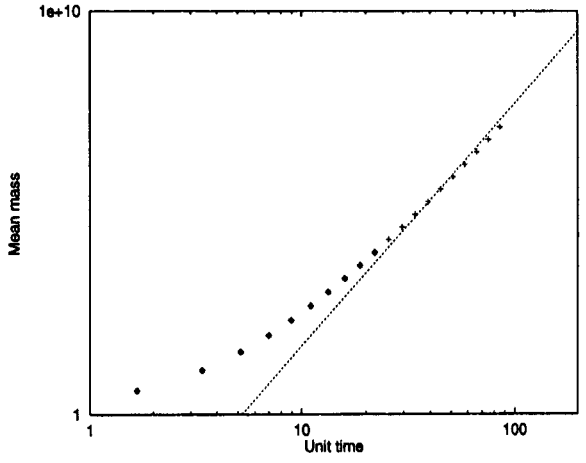

Figure 45:
Mean mass evolution for the same epochs as fig.44.

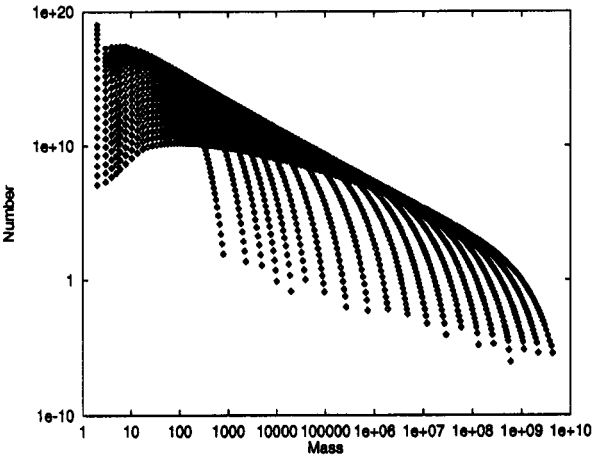

Figure 46:
Same as fig44, but for fractal growth

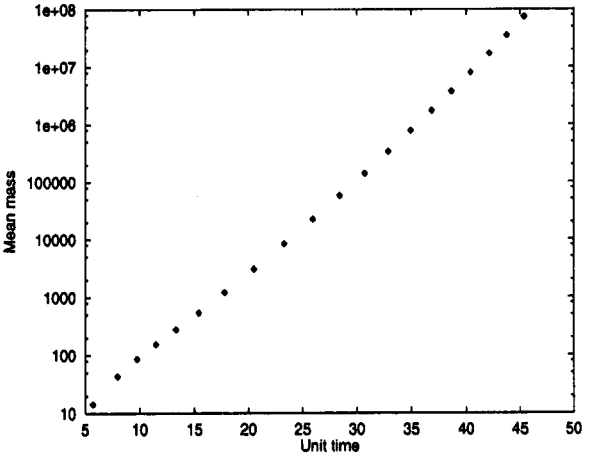

Figure 47:
Mean mass evolution for the same epochs as fig.46.

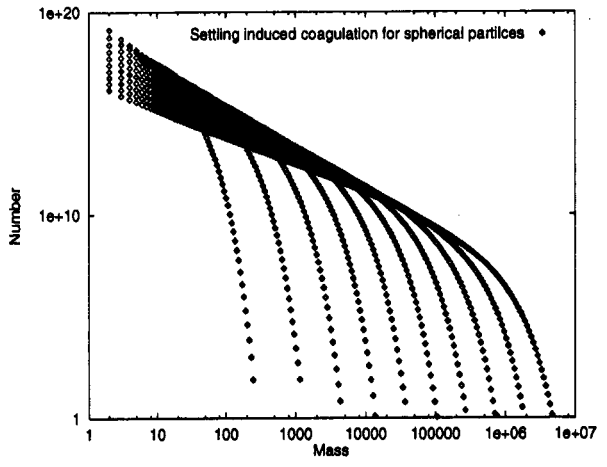

Figure 48:
Evolution of size distribution with settling kernel

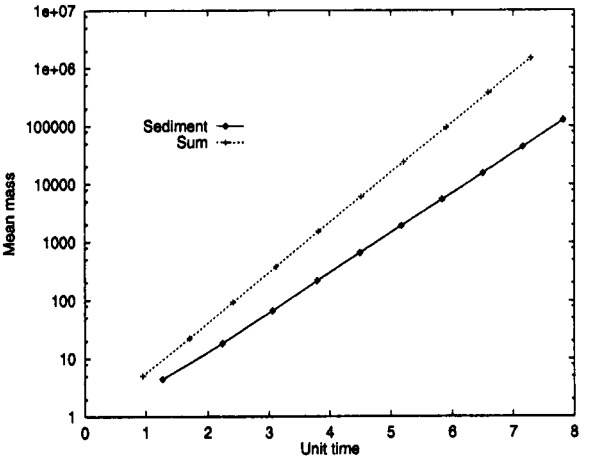

Figure 49:
Mean mass evolution for the same epochs as fig.48

between settling and growth accelerate this process. He estimated that centimeter-sized particles are formed in the midplane after several thousand years at 1 AU. However, we cannot estimate the spatial density of such "exceptionally large" particles or when such a feedback start to work in this picture.

Solving partial-differential equations for coagulation with settling (see section 4.1), Weidenschilling (1980) and Nakagawa et al. (1981) reached basically same conclusion as Safronov. But there exist an important quantitative difference between those two approaches. In the Safronov picture, it is implicitly assumed that total mass in the system is concentrated in small particles. On the other hand, in the settling-induced coagulation processes, total mass is dominated by larger particles at the exponential tail of the size distribution. Actually, Berry (1967) has shown that the growth speed for the Safronov picture ("continuous model" in terms of atmospheric sciences) is different from that for coagulation equation (denoted as "stochastic model" in his paper). Thus, the agreement between the results of numerical simulations and the estimate by Safronov might be a casual coincidence. One of main objects in this section is to verify this conjecture.

In order to generate dust layer with higher spatial density, dusty components mustbe separated from spatially uniform gas-dust mixture. Since we can regard the separation process as a pattern formation in the protoplanetary disk, it seems natural to expect the similarity between our problem and the reaction-diffusion systems, to which numerous theoretical and experimental studies of pattern formation have been devoted (Nicolis 1993, van Dongen 1988,1989 I,1990). Generally in the reaction-diffusion systems, the reaction rate is much smaller than diffusion rate before pattern formation. As we noted in section 4.1, this is a sufficient condition for mean-field approaches. Inhomogeneity appears when the system cross the critical point (Nicois and Progogine 1989) where

$$t_{reaction} = t_{diffusion} \tag{57}$$

In contrast, the time scale for coagulation (reaction) is much faster than settling (diffusion) time scale in the disk, at least in the beginning. But the coagulation time scale will becomes longer and the settling time scale shorter as the coagulation process continues. When $t_{coagulation}$ becomes longer than $t_{settling}$, the particles start to settle down from the system rather than grow at the original position.

Figure 50:

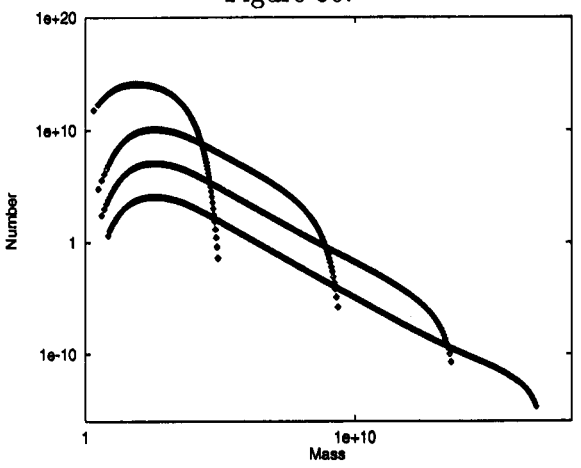

Evolution of size distribution with thermal motion and settling

Figure 51:

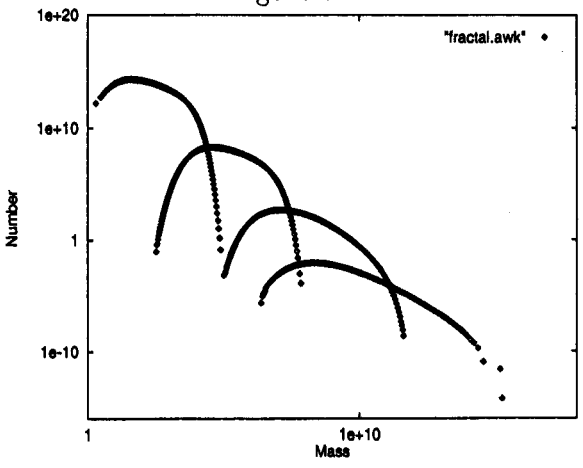

Same as fig. 50, but for fractal growth

Figure 52:

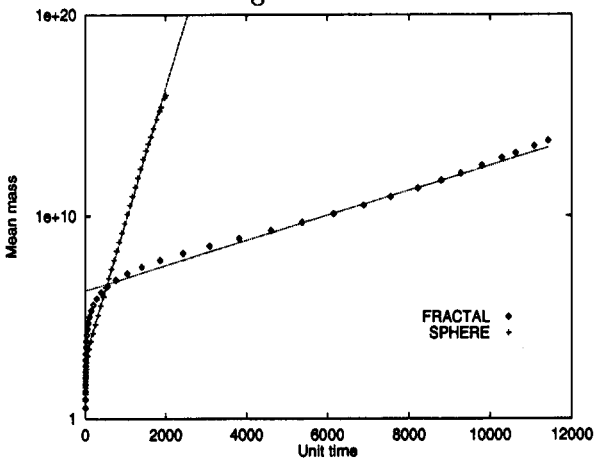

Comparison of the mean mass growth rate

Figure 53:

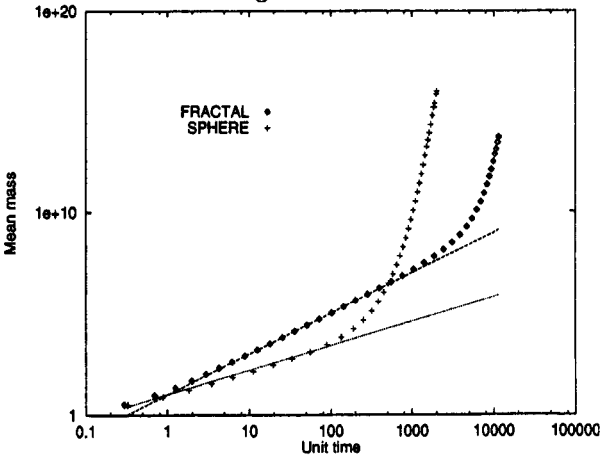

Same as fig. 52, but the horizontal axis is drawn with log scale

Thus, the condition for pattern formation can be formulated as

$$t_{coagulation} = t_{settling} \tag{58}$$

in analogy with reaction-diffusion system. Insofar as the theory of planet formation, only a few works paid attention to this simple, but profound condition which indicates the critical point for the structure formation. Comparing the time scale of coagulation with the settling time scale, Dubrulle et al. (1995) the critical size for dust sub-disk formation. However, their arguments includes an unrealistic assumption that only one coagulation time scale can represents the whole system. In our notation, it corresponds to the coagulation time scale for the mean mass in the system. An simple estimate is given by

$$\begin{aligned} t_{mean} = S/\dot{S} &\sim S^{1-\lambda} \quad \text{for } \lambda < 1 \\ &\sim \text{constant} \quad \text{for } \lambda = 1 \end{aligned} \tag{59}$$

In reality, the growth time scale varies with the size. The coagulation time scale for a dust particle of a given size k is defined as

$$t_k = N_k/(\sum_{i=1}^{\infty} K_{ki} n_i) \tag{60}$$

where the denominator represents the loss term in coagulation equation. We can calculate the quantity numerically for particles of any size in the simulation. On the other hand, settling time scale for a dust particle is estimated as a time required to transverse the system with the terminal velocity. Figures 54 and 55 compares the two time scales for spherical and fractal growth, respectively. The coagulation time scales are indicated for the same epochs as figs. 48 and 49. In order to calculate the settling time scale, thickness of the system must be specified. Followgin Nakagawa et al. (1981), we took the value for J zone located at the highest part of the disk. For spherical case, the growth mode changes from power-law to exponential immediately. After the transition, coagulation time scale becomes constant as shown by eq.60, except at the upper tail where the particles are most reactive and resulting in shorter growth time scale. Since larger particles settle faster, particles containing more than roughly 10^9 constituents ($\sim 1mm$) cannot stay in the system and begin to precipitate ($t_{growth} > t_{settling}$). As the system lies on the top of the disk, settling induced coagulation proceeds fastest here (see eq.54). Once larger particles settle down, they will continue settle and grow by sweeping up smaller particles in the lower part of the disk. This completely agree with the Safronov's picture. On the other hand, fractal growth stays longer at power-law stage, where $t_{mean} \sim S^{1-\lambda}$, then finally moves to exponential stage. From fig. 55, it is found that the time scale for coagulation is not significantly reduced compared with spherical growth, whereas settling time scale becomes much longer. The two lines never intersect in the mass range investigated here. Consequently, no settling occurs for fractal growth.

Now let us examine the spherical growth qualitatively. Nakagawa et al. reported that the mass transfer starts after 1000 years, whereas in our simulation only the largest batch has longer coagulation time than settling time scale even at 800 unit time ($\sim$ 6500 years). what is the reason for this discrepancy? Following two possibilities are considered:

1. if the initial particle number is much larger (10^{20} in our simulations), the upper tail of the size distribution gives much longer coagulation time scale and initiate the settling earlier.

2. if the thickness of the system size is smaller, the settling time scale can be reduced. This may result in faster onset of downward mass transfer.

Figure 54:

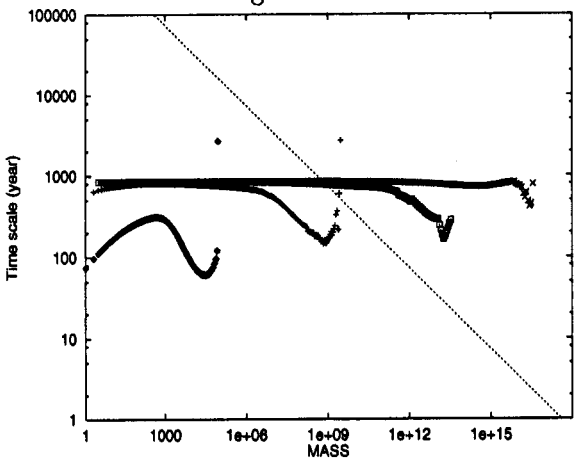

Comparison of the growth and settling time scale for spherical growth. Symbols indicates the coagulation time scales for the same epochs as in fig.50 A dotted line denotes the settling tiome scale as a function of the dust mass

Figure 55:

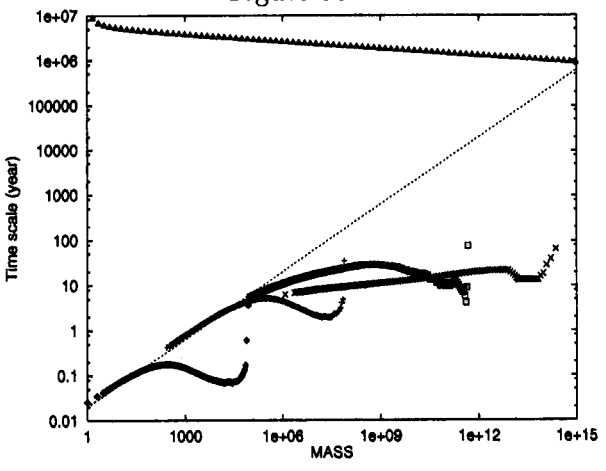

Same as fig. 54, but for fractal growth. Triangles are settling time scale and a dotted line is "mean" coagulation time scale defined by eq.(60) Note the difference in the size of a constituent partile and the unit time.

In any case, the important quantity is the system size, which is not explicitly specified in coagulation equation. Traditionally, the upper cut-off of the size distribution is determined arbitrary by non-physical requirements, such as computational convenience. The importance of the explicit system size was pointed out by Ohtsuki et al. (1990).They have shown that the unphysical tiny fraction at the upper tail of the size distribution requires unacceptably smaller time steps and may cause artificial acceleration of the growth. Similarly, the unphysical upper tail can initiate settling because the coagulation time scale for such region can be considerably long. (please extrapolate the time scale curves in figs. 54 and 55) And once Safronov scenario begins to work, localized structure cause rapid growth/settling as Nelson (1971) pointed out. It can be concluded that we must carefully account for the system size if we want to find the inhomogeneity onset.

Next, we will study another example which shows the importance of the explicit system size. When the partile grows larger than the mean free path of the gas molecules, the gas drag law changes from Epstein to Stokes. Under typical condition of the disk at 1 AU as tabulated in table 5, the Stokes drag regime ranges from centimeter(= mean free path) to approximately meter size for spherical compact dust particles. Since the Stokes drag is proportional to the radius rather than cross section of the particle, the coagulation kernel for spherical growth in this regime is

$$K_{ij} = (i^{1/3} + j^{1/3})^2 |i^{2/3} - j^{2/3}| \tag{61}$$

The exponent $\lambda = \nu = 4/3$ implies that this kernel leads to gelation (runaway growth). As we explained in section 4.3, our code can trace the evolution of gell mass (runaway body). We have found an unexpected bahaviour of the evolution of the mean mass. Figure 56 indicates the results of our calculations with this kernel. One can immediately see system size dependence of gelation (runaway) onset. The gelation occurs faster as the system size increases. Further, while the gell mass for product kernel increases gradually after the critical time ($t_c = 1$ in unit time), that for eq.61 absorb the total

mass in the system abruptly. Domilovskii et al. (1978) also claimed that gradient coagulation in a turbulent stream is described by eq.(61). On the basis of their MC simulations of random processes described by Master equation, they speculated that the critical time for gelation onset tends to zero as the system size is increased. Also, the MC simulations by Spouge (1985), based on Gillespi's rigorous algorithm, supports the possible occurrence of an instantaneous gelation transition. Wetherill (1990) also examined the runaway growth with the kernel proportional to $(i+j)^{4/3}$, but not mentioned the system size dependence. How can we understand these results?

Once a runaway body forms, simple coagulation equation is insufficient to describe the system evolution as we found in section 4.2. There exists mass flux from sol phase to gel phase. Consequently, we must take into account of the interaction between Sol (swarm) and Gel (Runaway body) with the physical modeling. As Wetherill (1990) did, the interaction can be modeled by adding an extra term $-K_{kG}N_kN_G$ to the r.h.s of coagulation equation. This heuristic model assumes that the gell is reactive as well as sol particles. More detailed analysis can be found in Ziff and Stell(1980) and Ziff et al. (1985). Present example corresponds to the kinetic F-model in terms of their classification of sol-gel interaction. Assuming the kernel is the homogeneous function as eq. 18, this additional term becomes

$$-k^{\mu}(k_G)^{\nu}N_kN_G = -k^{\mu}(k_G)^{\nu-1}N_kM_G \tag{62}$$

where $M_G = k_GN_G$ denotes the total gell mass. Despite of the finite total mass in the system, the gel is identified with an infinite cluster ($k_G = \infty$) in the coagulation equation (remember the divergence of M_2 moment). One finds from this expression that sol-gel interactions yield a finite, non-vanishing contribution to coagulation equation only if $\nu = 1$, as is the case for product kernel. If $\nu < 1$, the new term is zero, implying the original coagulation equation gives proper description of combined sol-gel system. For $\nu > 1$, the newly introduced interaction term is infinite, implying the instantaneous mass transfer from the sol to gel. Van Dongen (1987 I) have refined the above primitive argument and indicated that the critical time approaches infinitesimal for the kernel satisfying $\nu > 1$.

MC simulations and our calculations differs from coagulation equation in two respects. First, these calculations have been designed to simulate finite stochastic system described by Master equation, rather than coagulation equation (see eq.15 to remember what an approximation we used to transform Master equation to coagulation equation). Thus, the system size is explicitly taken into account in the schemes and upper cut-off of the size distribution is naturally derived. Secondly, the interaction between sol and gel is included in the simulations with no additional modeling a posteriori. Thus, we conclude that our simulations have faithfully exhibited intrinsic feature of the actual physical system, i.e., the stochastic process dependent on the system size. Although we have assumed in section 4.4 that the bahaviour of a small subsystem duplicates the whole system to justify the "topping" procedure, it is obviously wrong if $\nu > 1$.

Finally, we discuss the implication of the system size dependence for fractal growth. When we consider a fractal aggregates, it will enter Stokes regime much faster than a spherical compact particles of equivalent mass due to the fluffy structure. Many experimental and theoretical (Meakin et al. 1985, Rogak and Flagan 1990, Mountain et al. 1986) works have suggested that the Stokes drag on fractal aggregates can be represented by the "effective" radius of the aggregates. If this simple approximation can be applied, the exponent $\lambda = 2/D + (1 - 1/D)$ is obviously larger than unity. Once runaway growth starts, the particle grows by the collision with much smaller particle. This is the environment for BPCA and the dimension will increase to 3 rapidly. But λ is still larger than unity even for D=3.

Until the relative speed reach the limiting speed/place, the runaway particle keep on growing. To the author's knowledge, however, the studies of Stokes drag on fractal aggregates concern the case where the constituent particles are also in Stokes regime (Rogak and Flagan 1990). If the constituent is in the free molecule regime, (of course the whole aggregate is larger than mean free path) the reliability of the above-mentioned simple formula is uncertain. Probably, the study of the molecular flow in porous media can be applied to this regime.

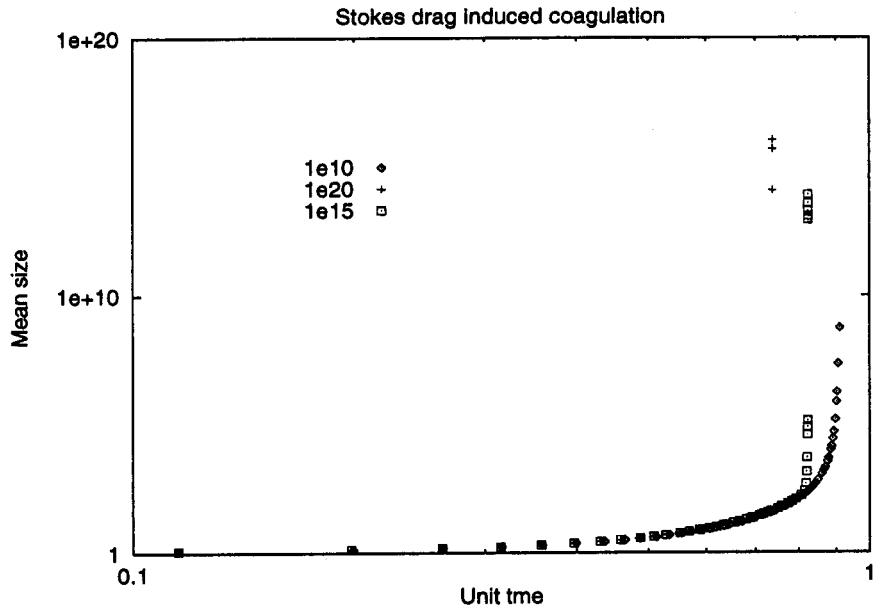

Figure 56: System size dependence of runaway onset

6 Future work

In this paper, we have attempted to investigate the coagulation of fractal aggregates with analytical and numerical calculations. On the other hand, there have been many experiments to study the aggregation processes. In spite of the variation of the chemical composition, such as soot (Samson et al. 1987), fumed silica (Schaefer and Hurd 1990) or metal oxides (Matsoukas and Friedlander 1991), these experiments verified that the formation of fractal aggregates is a universal phenomenon. Obviously, this fact has been the most strong motivation to introduce fractal concepts into the scenario of planet formation. Further advance of the theoretical approaches should be accompanied with the experiments. Actually, some of these experiments conducted in the free-molecule (Matsoukas and Friedlander 1991) or transition (Rogak and Flagan 1991.1993) regime may have direct astrophysical relevance and applicability. However, even with the small constituent particles, typically in the size range 2-10 nm, the aggregates grow to the sizes comparable to (or larger than) the mean free path of the gas molecules as coagulation proceeds. If the gas pressure is reduced to increase the mean free path, we cannot observe the coagulation process for sufficiently long period due to the rapid precipitation of large aggregates. An additional problem arising from gravity is the convective motion of the ambient gas which makes a exact estimates of collision rates very difficult (Higuchi and Sugiura 1993). In order to overcome these problems, a space experiment called CODAG is planned in near future (Keller et al.1993). The micro-gravity environment in the space station Columbus allow for low collisional velocities and a large Knudsen number of the surrounding gas. This experiment is expected to yield valuable information about the biggest unresolved problem in this field: i.e., the complexity of collisional outcome. We wish that our simulations will be used to , combined with the experimental data, give probability distribution for sticking, bouncing, fragmentation and restructuring dependent on the size and relative velocity of the collisional pair. The mechanical properties of fluffy aggregates, , such as the tensile strength or rigidity, are problems of significant importance relevant to not only dust, but also to planetesimal accumulation. A recent spectacular event, splitting of comet Shoemaker-Levy 9 by Jupiter's tidal force and the subsequent collision, strongly suggest that the cometary nucleus itself was the loosely bounded aggregates of sub-micron sized dust (Greenberg et al. 1995). In addition, new theory should address to the recent remarkable progress in observation of protoplanetary disk. In a wide range of wavelength, the structure and evolution of the protoplanetary disks have been revealed. Miyake and Nakagawa (1993,1995) investigated the evolution of T-Tauri stars spectrum based on the theory of dust growth in the surrounding disk.

Why don't we apply the same method to planetesimal accumulation? For example, Ziff (1980) mentioned the cosmological implications of the kernels with $\nu > 1$. Lushnikov (1978) also pointed out the relevance of gelation to gravitational coagulation. Although the coagulation equation has been a quite convenient and powerful approach, the capability is limited if one is interested in the emergence of the spatial structure because it includes mean-field assumption. In order to advance further beyond the mean-filed approximation, we must develop different methods. According to the suggestion by Sampson et al. (1986), the first alternative is numerical simulations of Master equation by statistically rigorous algorithm. The second methid to be considered is direct simulations of particle motion fully accounting for the movement of each particle in the system. Although the first approach is statistically complete and capable of treating considerable number of particles in a system, it shares the problems inherent to coagulation equation: i.e., no spatial information. The method of compounding moments, an extension of Master equation to incorporate spatial variations (van Kampen 1992, van Dongen 1991), cannot be used when the reaction (coagulation) time scale is faster than transport (diffusion or settling) time scale. Then, we should pursue the latter probability ,though computationally intensive.

Recent development of computer technology and code refinement enable us to solve a set of differential equations for all particles in a system. Using Box-tree-code, Ricahrdson (1995) investigated the dynamical behavior of spatially distributed particles with coagulation, bouncing and rotation. However, the sticking or bouncing probability is a parameter in his scheme. Sablotny et al. (1995) developed a code to simulate realistic aggregation processes with physical energy loss mechanisms upon collision. In order to take into account of the interaction of the surrounding gas, Mulholland et al. (1988) and Mountain et al. (1986) solved the Langevin equations for every particle in the system. But , the total number of particles is still too small to yield statistically reliable result in any scheme. In conclusion, three approaches, namely

The solutions of Coagulation equation
MC simulations based on Master equation
Direct Spatial simulations

must be developed together, complementing the disadvantage each other. In this sense, Wetherill scheme is a ideal hybrid of the former two approaches. Cellular automata (CA) models should be also pursued to compromise the heavy computational burden with higher spatial resolution (Karapiperis 1993). We plan to perform CA on one-dimensional lattice to simulate the settling-coagulation in the protoplanetary disk in near future.

Acknowledgement.

First of all, I greatly appreciate warm and continuing encouragement by Prof. T.Mukai. Also, I wish to thank Dr.Ohtsuki at Yamagata University because he kindly provided us the numerical code to solve coagulation equation and his related papers. Finally, I thank my colleagues in our lab: H.Ishimoto, H.Okamoto, H.Kimura and Y.Kitada for enlightening discussions. In particular, this paper wouldn't have been accomplished without close collaboration with *K.Masuda and K.Urasaki.* This work has been partially supported by the grant from JSPS.

References

[1] Adachi,Y and Ooi,S. J.Colloid Int.Sci., 135, 3374,1990

[2] Adachi,I., Hayashi,C. and Nakazawa, K. Prog.Theo.Phys.,56,1756,1976

[3] Allen,M.D., Raabe,O.G. J. Aerosol Sci., 16,57, 1985

[4] Baines,M.F., I.P.Williams, and A.S.Asebiomo MNRAS, 130, 63, 1965

[5] Ball,R.C.,Weitz,D.A.,Witten,T.A. and Leyvraz,F. Phys.Rev.Lett.,58,274,1987

[6] Bayewitz,M.H.,Yerushalmi,J.,Katz,S. and Shinnar,R. J.Atomos.Sci.,31,1604,1974

[7] Berry,E.X. J.Atomos.Sci.,24,688,1967

[8] Bleck,R. J.Geophysi.Res.,27,5165,1970

[9] Blum, J., Münch, M. Icarus ,106,151,1993

[10] Blum, J. Adv. Space Res. , 15, 10:39,1995

[11] Blum, J.,G.wurm,Kempf,S and Henning,Th personal communication

[12] Botet,R., Jullien,R. and Kolb,M. Phys.Rev.A., 30, 2150, 1984

[13] Bratley,P., Fox,B.L, ACM Trans. Math. Software 14, 88, 1988

[14] Broide,M.L. and Cohen, R.J. Phys.Rev.Lett., 64, 2026, 1990

[15] Brownlee,D. in : Interstellar Processes
eds. Hollenbach,D. and Thronson,H., Dordrecht:Reidel 1987 , p. 513

[16] ben-Avraham,D.,Burschka,M.A. and Doering,C.R. J.Stat.Phys.,60, 695,1990

[17] Cabane,M. et al. Planet. Space Sci., 41,257, 1993

[18] Chan.P,. B.Dahneke J.Appl.Phys., 52,3106, 1981

[19] Chen,Y, Yeh H. and Allen,M.D. Aerosol Sci. Tech., 14, 418, 1988

[20] Choksi, A., Tielens, A.G.G.M. and Hollenbach, D. Apj.,407,806,1993

[21] Dahneke,B.E. Aerosol Sci,. 4, 147, 1973

[22] Doering,C.R. and ben-Avraham,D. Phys.Rev.A., 38, 3035,1988

[23] Domilovskii, E.R., Lushnikov,A.A. and Piskunov,V.N. Dokl.Chem.Phys., 240, 108, 1978

[24] Dominik.C and Tielens,A.G.G.M Phil. Mag. A, 72, 783, 1995

[25] Donn,B. Astron.Astrophys., 235, 441, 1990

[26] Draine,B.T. in : Protostars and Planets II
eds. Black,D.C and Matthews,M.S, University Arizona presss p. 621

[27] Dubrulle,B., Morfill.G and Sterrzik,M Icarus ,114,237,1995

[28] Elminyawi,I.M., Gangopadhyay,S. and Sorensen,M J.Colloid Int.Sci., 144, 315,1991

[29] Frenklach,M. and Harris,S.J. J.Colloid Int.Sci., 118, 252,1987

[30] Fox,B.L. ACM Trans. Math. Software 12, 362, 1986

[31] Gay,J.G. and Berne,B.J. J. Colloid Interface Sci. 109, 90, 1986

[32] Gillespie,D.T J.Atmos.Sci., 29, 1496, 1972

[33] Gillespie,D.T J.Atmos.Sci., 32, 600, 1975

[34] Gillespie,D.T J.Comput.Phys., 22, 403 1976

[35] Gillespie,D.T J.Phys.Chem., 81, 2340, 1977

[36] Gillespie,D.T J.Comput.Phys., 22, 403 1976

[37] Gillespie,D.T Physica A., 188, 404, 1992

[38] Gillespie,D.T Markov Processes: An Introduction for Physica Scientists.
Academic Press, San Diego, 1992

[39] Gold,T. MNRAS, 112, 215, 1952

[40] Greenberg,J.M,Mizutani,H. and Yamamoto,T. Astron.Astrophys., in press 1995

[41] Gurav,A.et al Aerosol Sci. Tech., 19, 411, 1993

[42] Hayakawa,H J.Phys.A., 20, L801, 1987

[43] Hayakawa,H and Hayakawa,S Publ.Astron.Soc.Japan, 40, 341, 1988

[44] Hayashi,C. and Nakagawa,Y. Prog.Theo.Phys., 54, 93, 1975

[45] Hayshi,C.,Nakazawa,K and Nakagawa,Y. in : Protostars and Planets II
eds. D.C.Black and M.S.Matthews, University Arizona presss p. 1100

[46] Hendriks,E.M.,Ernst,M.H and Ziff,R.M. J.Stat.Phys.,31,519,1983

[47] Hendriks,E.M.Spouge,J.L.,Eibl,M and Schreckenberg,M Z.Phys.B., 58, 219,1985

[48] Higuchi, Y., Sugiura, N. Proc. Third Congress. Int on Optical Particle Sizing , pp. 217, 1993

[49] Hutchins,D.K. et al. Aerosol Sci. Tech., 22, 202, 1995

[50] Hong,S.S. and Greenberg,J.M Astron.Astrophys., 88, 194, 1980

[51] Jiang,Y. and Leyvraz,F. J.Phys.A,26, L179,1993

[52] Jiang,Y. and Leyvraz,F. Phys.Rev.E, 50, 2148, 1994

[53] Kang,K and Redner Phys.Rev.A.,30,2833,1984

[54] Kang,K.,Redner,S,Meakin,P and Leyvraz,F Phys.Rev.A.,33,1171,1986

[55] H.U.Keller et al. Adv.Space Res., 13, 73, 1993

[56] Kaplan,C.R. and Gentry,J.W. Aerosol Sci.Tech., 8, 1988

[57] Karapiperis,T. in : CELLULAR AUTOMATA — Prospects in Astrophysical Applications — eds. Perdang,J.M. and Lejune,A., World Scientific 1993, p. 187

[58] Keller,H.U., W.J.Markiewicz Geophys. Res. Lett., 18,249, 1991

[59] Lai,F.S.,Friedlander,S.K.,Pich,J. and Hidy,G.M. J.Colloid Int.Sci., 39, 395,1972

[60] Lapidus,A. and Shafrir,U J.Atomos.Sci.,29,1308,1972

[61] Leyvraz,F. in : On Growth and Form
eds. E.Stanley and N.Ostrowsky, Martinus Nijhoff Publisher 1986 p. 136

[62] Liffman,K. J. Comput. Phys. 100, 116, 1992

[63] Lissauer,J.J. and Stewart,G.R. in : Protostars and Planets III
eds. E.H.Levy, J.I.Lunine , University Arizona presss p. 1061

[64] Lushnikov,A.A. J.Colloid Int.Sci., 45, 549, 1973

[65] Lushnikov,A.A. J.Colloid Int.Sci., 65, 276, 1978

[66] Markiewicz,W.J., Mizuno,H., and Völk,H.J. Astron.Astrophys. 242, 286, 1991

[67] Mathis,J.S., Rumpl,W., Nordsieck,K.H. Apj.,217,425,1977

[68] Mathis,J.S in : Interstellar Dust
eds. Allamandola,L.J. and Tielens,A.G.G.M., KLUWER, p. 357-365

[69] Mizuno,H., Markiewicz,W.J, and Völk,H.J Astron. Astrophys. 242,286, 1991

[70] Matsuoukas and Friedlander,S.K. J.Colloid Int.Sci., 146,495, 1991

[71] Meakin,P. and B. Donn Apj 329, L39,1988

[72] Meakin,P. and Ernst,M.H. Phys.Rev.Lett., 60, 2503, 1988

[73] Meakin, P Rev. of Geophys. 29,317,1991

[74] Meakin, P., Chen,Z.Y. and Deutch,J.M. J.Chem.Phys., 82, 3786,1985

[75] Meakin, P. and Jullien,R. J.Chem.Phys., 89, 246,1988

[76] Meakin,P., B. Donn, and G.W.Mulholland Langmuir 5,510,1989

[77] Miyake,K. and Nakagawa, Y. Icarus 106, 20, 1993

[78] Miyake,K. and Nakagawa, Y. Apj., in press 1995

[79] Mizuno,H. Prog. Theor. Phys. Supplement 96, 121, 1988

[80] Mizuno,H. Icarus 80, 189, 1989

[81] Mizuno,H., Markiewicz,W.J., and Völk,H.J. Astron.Astrophys. 195, 183, 1988

[82] Mountain, R. D., Mulholland,G.W. and Baum,H. J.Colloid Interface Sci., 114, 67, 1986

[83] Mukai,T.,H.Ishimoto, T.Kozasa,J.Blum and J.M.Greenberg Astron.Astrophys. 262,315,1992

[84] Mulholland,G.W.,Samson,R.J.,Mountain, R.D. and Ernst,M.H. Energy and Fuels, 2, 481, 1988

[85] Mulholland,G.W. and Mountain,R.D. J.Chem. Phyis., 84, 4109

[86] Murthy,K.P.N J.Colloid Interface Sci., 119, 294, 1987

[87] Nakagawa,Y.,Nakazawa,K and Hayashi,C Icarus 45,517,1981

[88] Nakagawa,Y.,Sekiya,M.,Hayashi,C. Icarus 67 ,375,1986

[89] Nakamura,R, Kitada,Y. and Mukai,T Planet. Space Sci. 42, 721, 1994

[90] Nelson,L.D. J.Atoms.Sci., ,752 ,1971

[91] Nicolis,G Introduction to Nonlinear Science, Cambridge University Press, 1995

[92] Nicolis,G and Prigogine, I. Exploring Complexity — An Intoriduction,
R.Piper GmbH & Co,KG verlag, München , 1989

[93] Niederreiter,H. Bull.Am.Math.Soc., 84, 957, 1978

[94] Ohtsuki,K and Nakagwa,Y. Icarus 75,552,1988

[95] Ohtsuki,K., Nakagawa,Y. and Nakazawa,K. Icarus 83, 205, 1990

[96] Ossenkopf,V. A&A, 280, 617, 1993

[97] Pich,J. J.Colloid Int. Sci., 81,21,1969

[98] Praburam,G. and J.Goree ApJ 441,830 , 1995

[99] Press et al. Numerical Recipes in C, Cambridge University Press, 1991

[100] Pruppacher,H.R. and Klett,J.D Microphysics of Clouds and Precipitation,
Reidel Publishing, Dordrecht, 1978

[101] Purcell,E.M. Physica, 41,100, 1969

[102] Reid,G.C. J.Atmospheric Sci., 32,523,1975

[103] Richardson,D.C. Icarus, 115, 320, 1995

[104] Rogak,S.N., R.C.Flagan J.Colloid Int. Sci., 134, 206, 1990

[105] Rogak,S.N., R.C.Flagan J.Colloid Int. Sci., 151, 203, 1992

[106] Rogak,S.N., R.C.Flagan and H.V.Nguyen Aerosol Sci. Tech., 18, 25, 1993

[107] Ryan,B.F.,Shaw,D.E. and Simons,L. J.Atomos.Sci.,32,847,1975

[108] Sablotny, R.M., Kempf, S., Blum, J., Henning, Th. Adv. Space Res., 15, 10:55, 1995

[109] Safronov,V.S. Evolution of the protoplanetary cloud and formation of the Earth and the planets, NASA tech.trans. F-677. Nauka, Moscow, 1969

[110] Sampson,K.J. and Ramkrishna,D J.Colloid Interface Sci., 104, 269, 1985

[111] Sampson,K.J. and Ramkrishna,D J.Colloid Interface Sci., 110, 410, 1986

[112] Samson,R.J.,Mulholland,G.W. and J.W.Gentry Langmuir, 3 272, 1987

[113] Sarkar,P.K. and Prasad,M.A. J.Comp.Phys., 68, 66, 1987

[114] Seigneur,C et al. Aerosol Sci. Tech.,5,205,1986

[115] Seinfeld, J.H. Atmospheric Chemistry and Physics of Air Pollution., Jhon Wiley & Sons, New York, 1986

[116] Sekiya,M Prog. Theor. Phys. 69, 1116, 1983

[117] Simons,S. and Simpson,D.R. Ann.Nucl.Energy,16, 353, 1989

[118] Spouge,J.L. J.Colloid.Int.Sci.,107,38,1985

[119] Sutherland,D.N J.Colloid Interface Sci., 25, 373, 1969

[120] Sutherland,D.N and Goodarz-Nia,I. Chem.Eng.Sci., 26, 2071, 1971

[121] Takata,S. et al. Phys. Fluids A, 5, 716, 1993

[122] Tanaka,H. and Nakazawa,K. Icarus 107,404,1994

[123] Taylor, T.W. and Sorensen, C.M. Phys.Rev.A., 36, 5415, 1987

[124] Tohno,S. Aerosol Res., 10, 106, 1995

[125] Traub,J.F. and H.Wozniakowski Sci. Am. January 90, 1994

[126] van Dongen,P.G.J J.Phys.A,20,1889,1987

[127] van Dongen,P.G.J Physica. 145A, 15,1987

[128] van Dongen,P.G.J J.Stat.Phys.,49,927,1987

[129] van Dongen,P.G.J J.Stat.Phys.,53,221,1988

[130] van Dongen,P.G.J J.Stat.Phys.,54,221,1989

[131] van Dongen,P.G.J Phys.Rev.Lett.,63,1281,1989

[132] van Dongen,P.G.J J.Stat.Phys.,58,87,1990

[133] van Dongen,P.G.J and Ernst,M.H. Phys.Rev.Lett.,54,1396,1985

[134] van Dongen,P.G.J and Ernst,M.H. J.Phys.A. , 18, 2779, 1985

[135] van Dongen,P.G.J and Ernst,M.H. J.Colloid Int.Sci., 115, 27,1987

[136] van Dongen,P.G.J and Ernst,M.H. J.Stat.Phys.,49,879,1987

[137] van Dongen,P.G.J and Ernst,M.H. J.Stat.Phys.,59,295,1988

[138] van Kampen,N,G. Stochastic Processes in Physics and Chemistry
— Revised and Enlarged Version —, North Holland, 1992

[139] Vemury,S.Kusters,K.A. and Pratsisnis,S.E. J.Colloid Int.Sci., 165, 53,1994

[140] Völk,H.J., Jones,F.C., Morfill, G.E. and Röser,S. Astron.Astrophys. 85, 316, 1980

[141] Weidenschilling,S.J. in Meteorites and the Early Solar System
eds. J.F.Kerridge et al. , University Arizona presss p. 348

[142] Weidenschilling,S.J., Donn,B. and Meakin,P.
in The Formation and Evolution of Planetary Systems
eds. H.A.Weaver et al. 131-150, 1989

[143] Weidenschilling,S.J. and J.N.Cuzzi in : Protostars and Planets III
eds. E.H.Levy, J.I.Lunine , University Arizona presss p. 333

[144] Weidenshiilling,S.J. MNRAS,180,57,1977

[145] Weidenschiilling,S.J. Icarus 44, 172, 1980

[146] Weidenschiilling,S.J. Icarus 60, 553, 1984

[147] Wetherill,G.W. Icarus 88,336,1990

[148] Wetherill,G.W. and Stewart,G.R. Icarus 77,330,1989

[149] Williams,M.M.R. Ann.Nucl.Energy,17,161,1990

[150] Wright,H. and Ramkrishna,D. Phys.Rev.E., 47,3225,1993

[151] Wu,M.K. and Friedlander,S.K. J.Aerosol Sci.,24,273

[152] Xiong,Y. and Pratsinis,S.E. J.Aerosol Sci.,24,283

[153] Ying,R. and Peters,M.H. Aerosol Sci. Tech., 14, 418, 1991

[154] Ziff,R.M. and Stell,G J.Chem.Phys.,733492,1980

[155] Ziff,R.M. J.Stat.Phys., 23, 241,1980

[156] Ziff,R.M., McGrady,E.D. and Meakin,P J.Chem.Phys, 82, 5269, 1985